11 Time-Dependent Anisotropy Decays

In the preceding chapter we described the measurement and interpretation of steady-state fluorescence anisotropies. These values are measured using continuous illumination, and represent an average of the anisotropy decay by the intensity decay. The measurement of steady-state anisotropies is simple. However, interpretation of the steady-state anisotropies usually depends on an assumed form for the anisotropy decay, which is not observed in the experiment. Additional information is available from measurements of the time-dependent anisotropy, that is, the values of $r(t)$ following pulsed excitation. The form of the anisotropy decay depends on the size, shape, and flexibility of the labeled molecule. The measured decays can be compared with the decays calculated from various molecular models. Anisotropies decays can be measured using the time-domain (TD) or the frequency-domain (FD) method.

It is important to understand the factors which affect the anisotropy decays. For a spherical molecule the anisotropy is expected to decay with a single rotational correlation time (θ). Perhaps the most frequent interpretation of the correlation time is in terms of the overall rotational correlation time of a protein. The measured values of θ can be compared with the values predicted for a hydrated sphere of equivalent molecular weight (eq. 10.46). However, anisotropy decays are usually multi-exponential, which can be the result of numerous factors. Multi-exponential anisotropy decays are expected for non-spherical fluorophores or proteins. The correlation times in the anisotropy decay are determined by the rates of rotation about the various molecular axes. By examination of the correlation time it is sometimes possible to estimate the shapes of proteins.

In addition to shape, anisotropy decays are affected by the segmental flexibility of the macromolecule. For instance, tryptophan anisotropy decays of proteins frequently display correlation times that are too short to be due to rotational diffusion of the whole protein. These components are usually due to independent motions of the tryptophan residue within the protein or on the surface of the protein. The rates and amplitudes of tryptophan side-chain motions have been used to study the nanosecond dynamics of proteins. Anisotropy decays can also be affected by resonance energy transfer between the same type of fluorophore, that is, depolarization due to homotransfer.

Anisotropy decays of membrane-bound probes have been particularly informative. Membrane-bound probes often display unusual behavior in which the anisotropies do not decay to zero. This occurs because some probes do not rotate freely in membranes, at least not within the ns decay times of most fluorophores. The extent of rotation is often limited by the anisotropic environment of a membrane. The nonzero anisotropies at long times can be interpreted in terms of the order parameters of the membrane. In this chapter we present examples of simple and complex anisotropy decays to illustrate the information available from these measurements. In the following chapter we describe more advanced concepts in anisotropy decay analysis.

11.1. TIME-DOMAIN AND FREQUENCY-DOMAIN ANISOTROPY DECAYS

Suppose a fluorophore is excited with a pulse of vertically polarized light, and that it rotates with a single correlation time. The anisotropy decay is determined by measuring the decays of the vertically ($\parallel$) and horizontally ($\perp$) polarized emission. If the absorption and emission transition moments are colinear, the time-zero anisotropy is 0.4. In this case the initial intensity of the parallel component is threefold larger than that of the perpendicular component (Figure 11.1, left). If the fundamental anisotropy is greater than zero ($r_0 > 0$), vertically polarized excitation pulse results in an initial population of fluorophores which is enriched in the parallel orientation.[1] The decay of the differ-

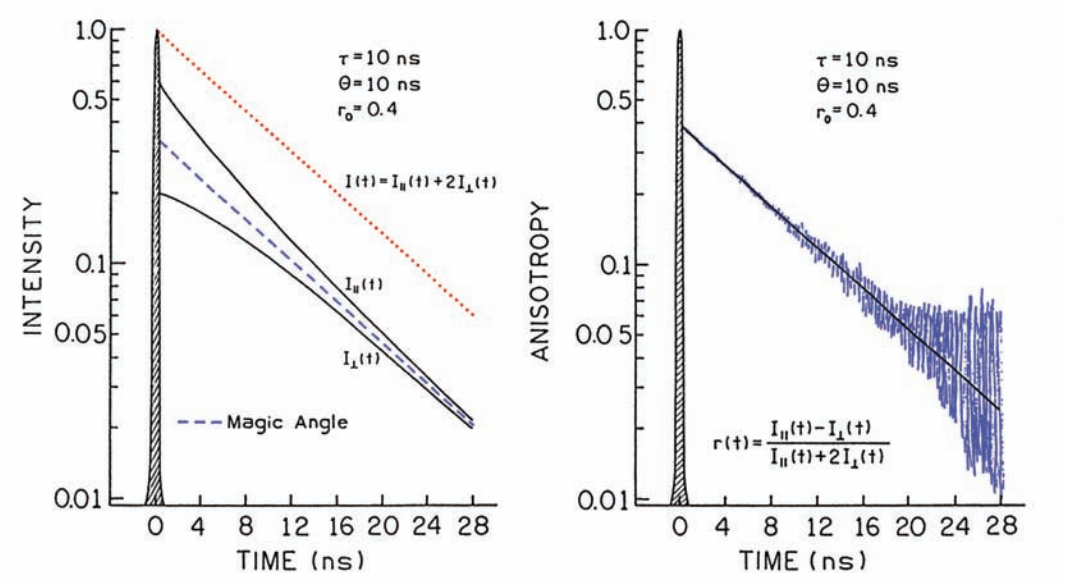

Figure 11.1. Time-dependent polarized decays (left) and the calculated anisotropy decay (right). From [1].

ence between $I_{\|}(t)$ and $I_{\perp}(t)$, when properly normalized by the total intensity and corrected for the instrument response function, is the anisotropy decay (right).

The left panel of Figure 11.1 shows that the parallel component initially decays more rapidly than the horizontal component. This occurs because the vertically oriented fluorophores are decaying by two processes: the intensity decay with decay time τ, and rotation out of the vertical orientation with correlation time θ. The horizontal component initially decays more slowly because it is repopulated by rotation from the excess vertically oriented population.

Suppose the sample displays a single lifetime and a single correlation time. Even under these conditions the polarized intensity decays are multi-exponential. The decays of the parallel (||) and perpendicular (⊥) components of the emission are given by

$$I_{\|}(t) = \frac{1}{3}I(t)\left[1 + 2r(t)\right] \tag{11.1}$$

$$I_{\perp}(t) = \frac{1}{3}I(t)\left[1 - r(t)\right] \tag{11.2}$$

where $r(t)$ is the time-resolved anisotropy. Generally, $r(t)$ can be described as a multi-exponential decay:

$$r(t) = r_0 \sum_j g_j \exp(-t/\theta_j) = \sum_j r_{0j} \exp(-t/\theta_j) \tag{11.3}$$

where $r_0 = \Sigma r_{0j}$ is the limiting anisotropy in the absence of rotational diffusion, the θ_j are the individual correlation times, and the g_j are the fractional amplitudes of each correlation time in the anisotropy decay ($\Sigma g_j = 1.0$). Depending on the circumstances, r_0 may be a known parameter, perhaps from a frozen solution measurement. Alternatively, all the amplitudes (r_{0j}) can be considered to be experimental variables so that $r_0 = \Sigma r_{0j}$ is a variable parameter. As shown in the previous chapter, the total intensity for a sample is given by $I_T = I_{\|} + 2I_{\perp}$. Similarly, the total (rotation-free) intensity decay is given by

$$I(t) = I_{\|}(t) + 2I_{\perp}(t) \tag{11.4}$$

Forming this sum eliminates the contributions of $r(t)$ to the total decay. In the time domain one measures the time-dependent decays of the polarized components of the emission (eqs. 11.1 and 11.2). The polarized intensity decays can be used to calculate the time-dependent anisotropy

$$r(t) = \frac{I_{\|}(t) - I_{\perp}(t)}{I_{\|}(t) + 2I_{\perp}(t)} \tag{11.5}$$

The time-dependent anisotropy decay are then analyzed to determine which model is most consistent with the data. However, it is preferable to directly analyze the polarized intensity decays (Section 11.22) rather than the anisotropy values calculated from the polarized intensity decays.

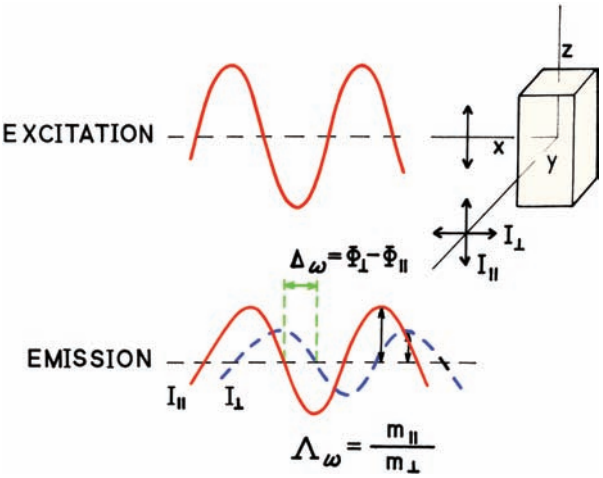

Figure 11.2. Frequency-domain measurements of anisotropy decays. For simplicity the average intensity is assumed equal for both polarized components. From [2].

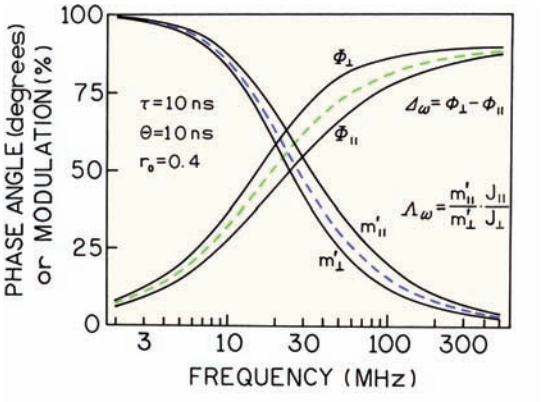

Figure 11.3. Simulated FD data for an anisotropy decay, τ = 10 ns and θ = 10 ns, showing the phase and actual modulation ($m_\parallel$' and $m_\perp$') of the polarized components of the emission, relative to the modulated excitation or scattered light. The dashed line shows the rotation-free phase and modulation values for the total emission. From [1].

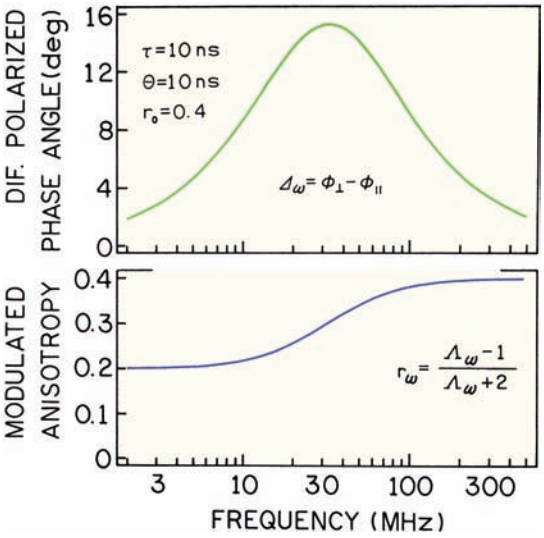

Figure 11.4. Differential phase (Δ_ω) and modulated (Λ_ω) anisotropy for τ = 10 ns, θ = 10 ns, and r_0 = 0.4. From [1].

The experimental procedures and the form of the data are different for frequency-domain of the anisotropy decay measurements.[2] The sample is excited with amplitude-modulated light, which is vertically polarized (Figure 11.2). The emission is observed through a polarizer that is rotated between the parallel and perpendicular orientations. In the frequency domain there are two observable quantities that characterize the anisotropy decay. These are the phase shift Δ_ω, at the modulation frequency ω, between the perpendicular ($\phi_\perp$) and parallel ($\phi_\parallel$) components of the emission:

$$\Delta_\omega = \phi_\perp - \phi_\parallel \tag{11.6}$$

and the ratio

$$\Lambda_\omega = m_\parallel / m_\perp \tag{11.7}$$

of the parallel ($m_\parallel$) and perpendicular ($m_\perp$) components of the modulated emission. To avoid confusion, we stress that Λ_ω is the ratio of the modulated amplitudes of the polarized components, not the ratio of the modulation of each polarized component. The ratio Λ_ω is often presented as the frequency-dependent anisotropy (r_ω), which is defined by

$$r_\omega = \frac{\Lambda_\omega - 1}{\Lambda_\omega + 2} \tag{11.8}$$

The form of the frequency-domain anisotropy data is illustrated in Figures 11.3 and 11.4. Analogous to the time-domain measurements, one could measure the phase and modulation of the polarized components relative to scattered light (Figure 11.3, solid lines). The phase angle of the parallel component ($\phi_\parallel$) will be smaller than the rotation-free phase angle for the total emission, and the modulation of the parallel component will be larger than that of the rotation-free modulation (dashed). These effects are the result of the shorter mean decay time of the vertically polarized decay (Figure 11.1). Similarly, the phase angle of the perpendicular component is larger, and the modulation smaller, because this component is being repopulated by the excess population in the parallel orientation, resulting in a longer mean decay time for the perpendicular component.

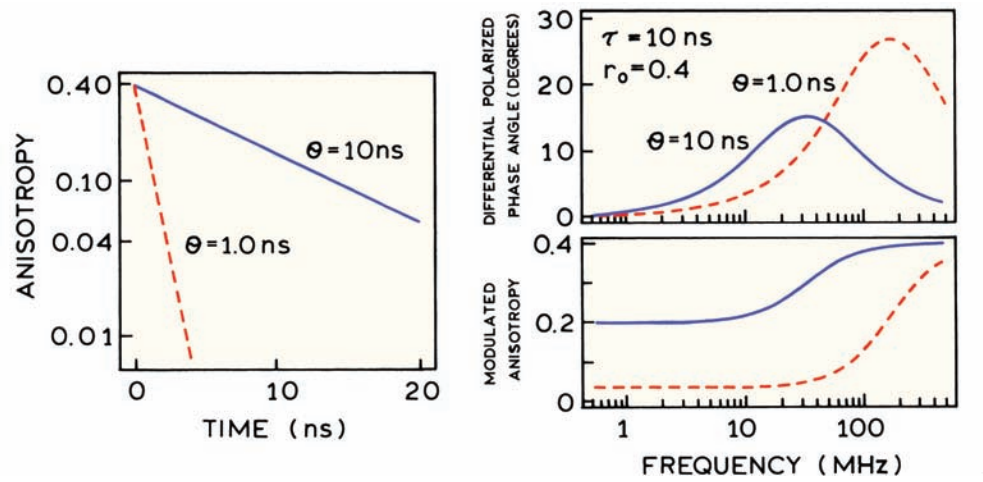

Figure 11.5. Comparison of TD and FD anisotropy decays with correlation times of 1.0 and 10.0 ns.

While the concept of a mean decay time is useful for understanding the relative behavior of the polarized intensity decays, the use of mean decay times to describe the decay times of the polarized components resulted in some confusion in the early literature.[3–6] For clarity we note that the modulations shown in Figure 11.3 ($m_{\parallel}'$ and $m_{\perp}'$), are the actual modulation of these components ($I_{\parallel}(t)$ and $I_{\perp}(t)$). For calculation of the anisotropy decay we use the non-normalized amplitudes of the modulated components of the polarized emission.

While one could measure $\phi_{\parallel}$, $\phi_{\perp}$, $m_{\parallel}'$, and $m_{\perp}'$ to obtain the anisotropy decay, this is not the preferred method. Almost all FD anisotropy decays are measured by the differential method. The differential polarized phase angle (Δ_{ω}) and modulation ratio (Λ_{ω}) is measured directly by rotation of the emission polarizer. It is more accurate to measure the difference and ratio directly, rather than calculating these values from two independently measured values.

The differential form of the FD anisotropy data measured by the differential method is illustrated in Figure 11.4. The differential phase angles appear to be approximately Lorentzian in shape on the log-frequency scale. The modulated anisotropy increases monotonically with frequency. The value of r_{ω} at low frequency is equal to the steady-state anisotropy:

$$r = \frac{r_0}{1 + \tau/\theta} = \frac{r_0}{2} \qquad (11.9)$$

The low-frequency anisotropy of $r = 0.5\ r_0$ is a result of $\tau = \theta$ for the simulated curves. At high frequency, r_{ω} approaches r_0. Longer correlation times shift the Δ_{ω} and r_{ω} curves to lower modulation frequencies, and shorter correlation times shift these curves to higher frequencies.

It is valuable to visualize how changes in the anisotropy decay affect the TD and FD data. Suppose the correlation time decreases from 10 to 1.0 ns. In the TD data the anisotropy decays more rapidly (Figure 11.5). The changes in the FD data are somewhat more complex. The differential phase-angle distribution shifts to higher frequencies with shorter correlation times. The maximum differential phase angle increases or decreases depending on the relative values of τ and θ. A decrease in correlation time results in a decrease in the modulated anisotropy. The limiting value of r_{ω} at low frequency is the steady-state anisotropy, and at high frequency the limit is still r_0.

Suppose the anisotropy decays with two correlation times. A typical anisotropy decay for a protein would be a 5-ns correlation time for overall rotational diffusion and a 50-ps correlation time due to segmental motion of the tryptophan residue (Figure 11.6). The TD anisotropy shows a rapid decay due to the 50-ps component, followed by a slower decay at longer times. Depending upon the resolution of the TD instrument, the fast component may or may not be resolved in the measurements. However, the presence of the fast component can be determined from a time-zero anisotropy ($r(0)$), which is smaller than r_0.

The presence of two decay times also has an effect on the FD anisotropy data (Figure 11.7). Instead of a single Lorentzian distribution for Δ_{ω}, the differential phase angles show two such distributions, one for each correlation time (dashed lines). The presence of the rapid motion is evident

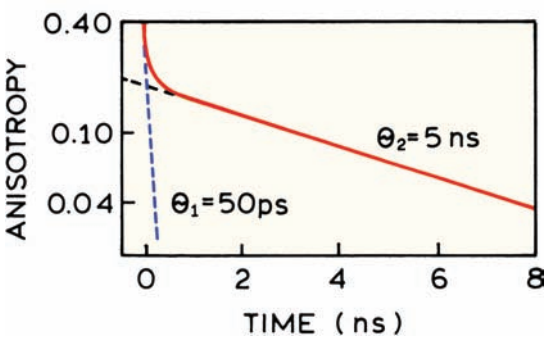

Figure 11.6. Simulated time anisotropy decay for a double exponential decay with $r_{01} = r_{02}$, $\theta_1 = 50$ ps, and $\theta_2 = 5$ ns.

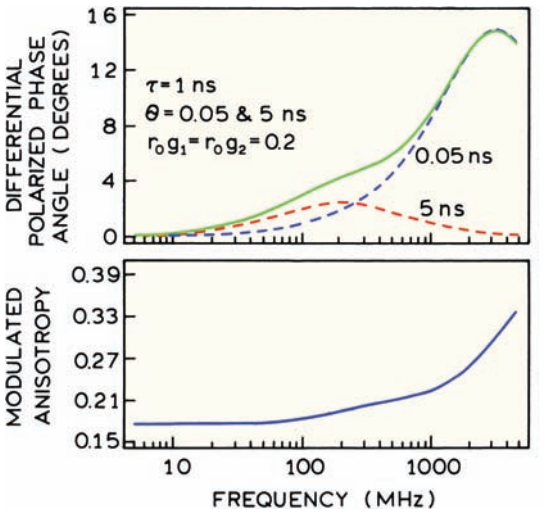

Figure 11.7. Frequency-domain anisotropy data for a double-exponential anisotropy decay. Revised from [2].

from the increasing phase angle at higher frequencies. If the amplitude of this rapid motion is increased, the phase angles become smaller at low frequencies and larger at the higher frequencies. If the rapid correlation time is very short, the frequency range of the instrument may not be adequate to detect this rapid motion. Then the increase in the differential phase angle at high frequency would not be observed. The emission may be highly demodulated due to the intensity decay, in which case the high-frequency limit of r_ω cannot be measured even if the instrument can measure at the higher frequencies. The presence of an unresolved motion can be detected by a failure of r_ω to approach the expected limiting value of r_0. This illustrates the advantage of using both the differential phase (Δ_ω) and modulation (r_ω) data in any attempt to resolved a complex and/or rapid anisotropy decay. A failure of r_ω to reach r_0 in the frequency domain is similar to finding $r(0) < r_0$ in the time-domain data. As for the intensity decays, the parameters describing the anisotropy decay are recovered by comparison of the data with calculated values obtained using various models.

One may notice that the lifetime is included in the FD anisotropy simulations (Figure 11.7), but not in the TD simulations (Figure 11.6). The FD data depend on the intensity decay time. In the time domain the anisotropy decays do not depend on the lifetime. However, the lifetime determines the time range over which the intensities can be measured.

11.2. ANISOTROPY DECAY ANALYSIS

11.2.1. Early Methods for Analysis of TD Anisotropy Data

The most direct approach to analyzing the anisotropy data is to fit the measured $r(t)$ values to an assumed anisotropy decay law. This approach is direct but partially incorrect. The measured values are calculated from the polarized intensity decays:

$$r_m(t_k) = \frac{N_\parallel(t_k) - GN_\perp(t_k)}{N_\parallel(t_k) + 2GN_\perp(t_k)} = \frac{D_m(t_k)}{S_m(t_k)} \qquad (11.10)$$

where the $N_\parallel(t_k)$ and $N_\perp(t_k)$ are the experimental data convolved with the instrument response function at time t_k; $D_m(t_k)$ is the difference between the polarized decays, and $S_m(t_k)$ is the total decay, both corrected using the G factor. The calculated values $r_m(t_k)$ are then compared with calculated values obtained from the convolution integral:

$$r_c(t_k) = \sum_{t=0}^{t=t_k} L(t_k) r(t - t_k) \Delta t \qquad (11.11)$$

where $L(t_k)$ is the instrument response function. The IRF is assumed to be independent of the orientation of the emission polarizer. The anisotropy decay is then determined by minimizing

$$\chi_R^2 = \frac{1}{\nu} \sum_{k=1}^{n} \frac{1}{\sigma_{Rk}^2} [r_m(t_k) - r_c(t_k)]^2 \qquad (11.12)$$

In this equation $r_c(t_k)$ is the anisotropy calculated using eq. 11.11 and the assumed anisotropy decay law, and ν is the number of degrees of freedom. The noise in the measurements does not decrease when taking the differences in the intensity values. Instead, the calculated anisotropy values

contain all the noise present in the measured polarized decays, and it is important to correctly propagate the noise. In this case the weighting factor is a moderately complex function of the counts in each channel,[7–8] and is given by

$$\sigma_{Rk}^2 = r_m^2(t_k)\left(\frac{\sigma_{Sk}^2}{S_m^2(t_k)} + \frac{\sigma_{Dk}^2}{D_m^2(t_k)} - \frac{2\sigma_{SDk}^2}{S_m(t_k)D_m(t_k)}\right) \quad (11.13)$$

where

$$\sigma_{Dk}^2 = N_{\parallel}(t_k) + G^2N_{\perp}(t_k) \quad (11.14)$$

$$\sigma_{Sk}^2 = N_{\parallel}(t_k) + 4G^2N_{\perp}(t_k) \quad (11.15)$$

$$\sigma_{SDk}^2 = \sigma_{Sk}^2 - 2G^2\sigma_{Dk}^2 \quad (11.16)$$

These expressions seem complex, but their origin is simple. These expressions are the result of propagating of the Poisson noise in each measured intensity into the anisotropy function. The origin of eq. 11.14 can be seen by considering the Poisson noise in the parallel and perpendicular components, which are given by $[I_{\parallel}(t_k)]^{1/2}$ and $[I_{\perp}(t_k)]^{1/2}$, respectively. The noise in the sum is given by the sum of the squares of the Poisson noise, with appropriate weighting by the G factor. The principles of error propagation can be found elsewhere.[9]

Anisotropy decays are sometimes analyzed by separate analysis of the sum and difference decays (eq. 11.10). In this method the sum $S_m(t_k)$ is analyzed first to obtain the parameters describing the intensity decay, which are the α_i and τ_i values when using the multi-exponential model. For this analysis χ_R^2 is minimized using

$$\chi_R^2 = \frac{1}{\nu}\sum_{k=1}^{n}\frac{1}{\sigma_{Sk}^2}[S_m(t_k) - S_c(t_k)]^2 \quad (11.17)$$

where σ_{Sk}^2 is given by eq. 11.15.

The intensity decay also appears in the difference data. The parameters (α_i and τ_i) recovered from the sum analysis are held constant during analysis of $D_m(t_k)$. Once again, χ_R^2 is minimized using[8,10]

$$\chi_R^2 = \frac{1}{\nu}\sum_{k=1}^{n}\frac{1}{\sigma_{Dk}^2}[D_m(t_k) - D_c(t_k)]^2 \quad (11.18)$$

where σ_{Dk}^2 is given by eq. 11.14. When this procedure is used the different $D(t)$ contain both the intensity decay and the anisotropy decay parameters. This can be seen by considering a single exponential decay of the intensity and the anisotropy. In this case

$$D(t) = S(t)r(t) = k\ \exp\left[-t\left(\frac{1}{\tau} + \frac{1}{\theta}\right)\right] \quad (11.19)$$

where k is a constant. Hence the difference $D(t)$ decays with an apparent decay time that is shorter than the lifetime (τ) and the correlation time (θ).

Of the two procedures described above, the second using separate analyses of $S(t)$ and $D(t)$ is preferable. This is because the use of eq. 11.10 to calculate the anisotropy is not correct, particularly when the correlation times are close to the width of the instrument response function. The operations of convolution and division do not commute, so that the measured values of $r_m(t_k)$ are not a convolution of the impulse response $r(t)$ with the lamp function. For instance, even if the anisotropy decay is a single exponential, the calculated values of $r_m(t_k)$ can display unusual shapes, particularly near the rising edge of the curve. Also, the apparent time-zero anisotropies $r(0)$ are often less than the true value of r_0.[11] The use of the calculated sum $S_m(t_k)$ and difference ($D_m(t_k)$) curves is more correct because the operations of addition and subtraction commute with convolution. However, this method still assumes that the lamp function is the same for the parallel and perpendicular components of the emission.

11.2.2. Preferred Analysis of TD Anisotropy Data

The preferred method of analysis is to directly analyze the polarized intensity decays without calculation of $r_m(t_k)$ or $D_m(t_k)$.[12–15] This is a form of global analysis in which the parallel and perpendicular components (eqs. 11.1 and 11.2) are analyzed simultaneously to recover the intensity and anisotropy decay law. The polarized decay laws are used with the instrument response function to calculate

$$N_{\parallel}^c(t_k) = \sum_{t=0}^{t=t_k} L_{\parallel}(t_k)I_{\parallel}(t - t_k)\Delta t \quad (11.20)$$

$$N_{\perp}^c(t_k) = \sum_{t=0}^{t=t_k} L_{\perp}(t_k)I_{\perp}(t - t_k)\Delta t \quad (11.21)$$

where $L_{\parallel}(t_k)$ and $L_{\perp}(t_k)$ are the instrument response func-

tions measured for each polarized component. In contrast to the previous method, the instrument response functions are not assumed to be identical for each polarization, and can be rather different without affecting the validity of the procedure.

The calculated and measured polarized intensities are then used to minimize χ_R^2 based on the parameter values in the intensity (α_i and τ_i) and anisotropy decays (r_{0i} and θ_i):

$$\chi_R^2 = \frac{1}{\nu}\sum_{t=0}^{n}\frac{1}{\sigma_{\|k}^2}\left[N_{\|}(t_k) - N_{\|}^c(t_k)\right]^2 + \frac{1}{\nu}\sum_{t=0}^{n}\frac{1}{\sigma_{\perp k}^2}\left[N_{\perp}(t_k) - N_{\perp}^c(t_k)\right]^2 \qquad (11.22)$$

Since the polarized intensity decays are used directly, the weighting factors are given by

$$\sigma_{\|k}^2 = N_{\|}(t_k) \qquad (11.23)$$

$$\sigma_{\perp k}^2 = N_{\perp}(t_k) \qquad (11.24)$$

There is no need to propagate the weighting factors into the sum and difference data. All the parameters are varied simultaneously to obtain the best fit, so that the intensity and anisotropy decay parameters are all optimized to match the actual data.

Sometimes it is necessary to correct the polarized intensity decays for background signals. The counts measured for the blank sample with each polarizer position are subtracted from the measured data for the same polarizer position:

$$I_{\|}(t_k) = I_{\|}(t_k)_{\text{sample}} - I_{\|}(t_k)_{\text{background}} \qquad (11.25)$$

$$I_{\perp}(t_k) = I_{\perp}(t_k)_{\text{sample}} - I_{\perp}(t_k)_{\text{background}} \qquad (11.26)$$

The weighting factor for the corrected data is given by the sum of the weighting factors for the sample and for the background. If the number of background counts is small, this correction to the weighting factor can be ignored. It is important to measure the background for both polarized components, because the background can be different for each component, particularly if scattered light reaches the detector.

It is necessary to know the G factor in order to calculate the intensity decay. The G factor can be obtained in the usual manner (Chapter 10), in which the intensities are measured with horizontally polarized excitation. The parallel and perpendicular intensities are then measured for the same period of time, assuming the excitation intensity is constant. Another method is to measure the steady-state anisotropy of the sample, which is then used to constrain the total intensities of the polarized decays. The steady-state anisotropy can be measured on a different instrument. The G factor can be calculated using[10,12]

$$G = \frac{1 - r}{1 + 2r}\frac{\sum N_{\|}(t_k)}{\sum N_{\perp}(t_k)} \qquad (11.27)$$

where the sums are the total number of counts in the polarized intensity decays. If the excitation intensity has changed, or the counting time is different, these values need to be corrected for the different experimental conditions.

11.2.3. Value of r_0

In the anisotropy decay analysis the value of r_0 can be considered to be a known or unknown value. If the value of r_0 is known, the anisotropy decay law can be written as

$$r(t) = r_0\sum_j g_j \exp(-t/\theta_j) \qquad (11.28)$$

where g_j are the fractional amplitudes that decay with the correlation times θ_j. Since $\Sigma g_j = 1.0$, the use of a known r_0 value reduces the number of variable parameters by one. In this type of analysis the time-zero anisotropy is forced to be equal to r_0.

Alternatively, the total or time-zero anisotropy can be a variable parameter. In this case,

$$r(t) = \sum_j r_{0j} \exp(-t/\theta_j) \qquad (11.29)$$

where r_{0j} are the fractional anisotropies that decay with correlation times θ_j. When using this type of analysis it is preferable to describe the time-zero anisotropy as $r(0)$, which is the recovered value of $t = 0$. If the anisotropy decay contains fast components that are not resolved by the instrument then the $\Sigma r_{0j} = r(0)$ is less than the fundamental anisotropy r_0.

11.3. ANALYSIS OF FREQUENCY-DOMAIN ANISOTROPY DECAYS

Analysis of the FD anisotropy data is performed in a manner similar to the intensity decay analysis (Chapter 5). There is a somewhat more complex relationship between the data (Δ_ω and Λ_ω) and the transforms. The calculated values ($\Delta_{c\omega}$ and $\Lambda_{c\omega}$) can be obtained from the sine and cosine transforms of the individual polarized decays:[3,16–17]

$$N_k = \int_0^\infty I_k(t) \sin\omega t\, dt \tag{11.30}$$

$$D_k = \int_0^\infty I_k(t) \cos\omega t\, dt \tag{11.31}$$

where the subscript k indicates the orientation, parallel (||) or perpendicular (⊥). For any assumed parameters the values Δ_ω ($\Delta_{c\omega}$) and Λ_ω ($\Lambda_{c\omega}$) can be calculated (subscript *c*) using the sine and cosine transforms of the polarized decays (eqs. 11.30 and 11.31). The calculated values of Δ_ω and Λ_ω are given by

$$\Delta_{c\omega} = \arctan\left(\frac{D_\parallel N_\perp - N_\parallel D_\perp}{N_\parallel N_\perp + D_\parallel D_\perp}\right) \tag{11.32}$$

$$\Lambda_{c\omega} = \left(\frac{N_\parallel^2 + D_\parallel^2}{N_\perp^2 + D_\perp^2}\right)^{1/2} \tag{11.33}$$

where N_i and D_i are calculated at each frequency. The parameters describing the anisotropy decay are obtained by minimizing the squared deviations between measured and calculated values, using

$$\chi_R^2 = \frac{1}{\nu}\sum_\omega \left(\frac{\Delta_c - \Delta_{c\omega}}{\delta\Delta}\right)^2 + \frac{1}{\nu}\sum_\omega \left(\frac{\Lambda_\omega - \Lambda_{c\omega}}{\delta\Lambda}\right)^2 \tag{11.34}$$

where $\delta\Delta$ and $\delta\Lambda$ are the uncertainties in the differential phase and modulation ratio, respectively.

In the FD analysis the rotation-free intensity decay is measured in a separate experiment using magic-angle polarizer conditions. The parameter values, typically α_i and τ_i for the multi-exponential model, are held constant during the calculation of χ_R^2 for eq. 11.34. In principle, the phase and modulation of the polarized components could be measured relative to scattered light (Figure 11.4), and the values used to recover $I(t)$ and $r(t)$. This would be analogous to the method used for TCSPC data. However, it appears that the anisotropy decay is better determined by direct measurement of the difference (Δ_ω) and ratio (Λ_ω) values.

There is no mention of the *G* factor in eqs. 11.30–11.33. This is because using the *G* factor is often unnecessary in analysis of the time-resolved data. This is because TD and FD measurements are typically performed using emission filters rather than a monochromator. The use of an emission monochromator in the steady-state anisotropy measurements is the dominant reason for the *G* factor being different from unity. For many time-resolved instruments, especially those using MCP-PMT detectors, the detection efficiency is the same for the parallel and perpendicular components, and hence $G = 1.0$.

In the frequency-domain measurements one checks for a sensitivity to polarization by excitation with horizontally polarized light. The measured values of the differential polarized phase angle (Δ_ω) should be zero. Also, the measured value of the modulation ratio (Λ_ω) should be 1.0. If needed, FD anisotropy decays can be measured in a T format to avoid rotation of the emission polarizer.[18]

When the FD anisotropy data are analyzed using eq. 11.34, the weighting factors are the same as those used for directly measured phase and modulation values. We find values of $\delta\Delta_\omega = 0.2$ and $\delta\Lambda_\omega = 0.004$ to be appropriate for measurements. For separately measured the polarized phase ($\phi_\parallel$ and $\phi_\perp$) and modulation ratios ($m_\parallel$' and $m_\perp$') it would be necessary to propagate the uncertainties into the difference and ratio files, as was done for the time-domain analyses. A procedure to correct for background fluorescence has been described for the frequency-domain anisotropy measurements.[19] This procedure is somewhat more complex than the direct subtraction used for the time-domain data.

The values of r_0 and $r(0)$ are also treated the same way in the FD analysis as in the TD analysis. The value of r_0 can be a fixed parameter (eq. 11.28), or the time-zero anisotropy ($r(0)$) can be a variable in the analysis (eq. 11.29). Using a fixed value of r_0 avoids the problem of missing a short correlation time present in the sample. However, use of an inappropriately large value of r_0 will result in the appearance of a short correlation time in the calculated anisotropy decay which is not present in the sample.

11.4. ANISOTROPY DECAY LAWS

Depending upon the size and shape of the fluorophore, and its local environment, a wide variety of anisotropy decays

are possible. A spherical molecule displays a single rotational correlation time. Anisotropy decays can be more complex if the fluorophore is non-spherical, or if a non-spherical molecule is located in an anisotropic environment. Another origin of complex anisotropy decays is internal flexibility of a fluorophore within a larger macromolecule.

11.4.1. Non-Spherical Fluorophores

One origin of multiple correlation times is a non-spherical shape. If a molecule is not spherical, there are different rotational rates around each axis. For instance, perylene is a disk-like molecule and the in-plane rotations are expected to be more rapid than the out-of-plane rotations. The out-of-plane motion requires displacement of solvent molecules. The in-plane rotations require less displacement of solvent and are expected to be more rapid. Such a molecule is referred to as an anisotropic rotor. Generally, macromolecules are nonsymmetric and one expects different rotational diffusion rates about each axis.

The theory for rotational diffusion of anisotropic rotors is complex. This topic is well understood, and is described in more detail in Chapter 12. Initially there was some disagreement about the predicted time-resolved decays for anisotropic molecules.[20–25] It is now agreed[20] that the anisotropy is expected to decay as a sum of exponentials:

$$r(t) = \sum_{j=1}^{5} r_{0j} e^{-t/\theta_j} \tag{11.35}$$

There may be as many as five exponential terms for an asymmetric body, but in practice only three correlation times are expected to be distinguishable.[25] Ellipsoids of revolution are elongated (prolate) or flattened (oblate) molecules with two equal axes and one unique axis. The anisotropy decay of ellipsoids of revolution can display only three correlation times. The values of r_{0j} and θ_j are complex functions of the rates of rotation around the molecular axes of the nonsymmetric body and the orientation of the absorption and emission dipoles relative to these axes. In practice, it is difficult to resolve more than two correlation times. It is important to remember that anisotropic rotations can result in multi-exponential decays of anisotropy. For small molecules in solution the rotational rates around the different axes are rarely different by more than a factor of ten. The resolution of such similar rates is difficult but has been accomplished using TD and FD measurements. The theory of anisotropic rotational diffusion is described in Chapter 12, along with examples resolving multiple correlation times.

It is important to remember that the theory for rotation of non-spherical molecules assumes hydrodynamic behavior, in which the rates of rotation are determined by the viscous drag of the solvent. This theory fails for many small molecules in solution. This failure occurs because small molecules can slip within the solvent, particularly if the motion does not displace solvent or if the molecule is not hydrogen bonded to the solvent. In these cases one can recover a multi-exponential anisotropy decay, but the values of r_{0j} and θ_j may not be understandable using eq. 11.35 with values or r_{0j} and θ_j appropriate for hydrodynamic rotational diffusion (Chapter 12). It is useful to have a definition for the mean correlation time. The most commonly used average is the harmonic mean correlation time, θ_H, which is given by

$$\frac{1}{\theta_H} = \frac{\sum_j r_{0j}/\theta_j}{\sum_j r_{0j}} = \frac{1}{r_0}\sum_j \frac{r_{0j}}{\theta_j} \tag{11.36}$$

This expression is sometimes used with $r(0)$ in place of r_0. For a non-spherical molecule, the initial slope of the anisotropy decay is determined by the harmonic mean correlation time.[26]

11.4.2. Hindered Rotors

Decays of fluorescence anisotropy can be complex even for isotropic rotors, if these molecules are contained in an anisotropic environment. For example, the emission dipole of DPH is oriented approximately along its long molecular axis. The rotations that displace this dipole are expected to be isotropic (Chapter 12) because the molecule is nearly symmetrical about this axis. Rotation about the long axes of the molecule is expected to be faster than the other rotational rates, but this fast rotation does not displace the emission dipole and hence does not depolarize the emission. Hence, only rotation that displaces the long axis of DPH is expected to depolarize the emission. In solvents only a single type of rotational motion displaces the emission dipole of DPH, and its anisotropy decay is a single exponential.

When DPH is in membranes the anisotropy decay is usually complex.[27–30] The rotational motions of DPH are hindered and the anisotropy does not decay to zero. By hindered we mean that the angular range of the rotational

motion is limited. In such cases a limiting anisotropy (r_∞) is observed at times which are long compared to the fluorescence lifetime. The anisotropy decay is described by

$$r(t) = (r_0 - r_\infty) \exp(-t/\theta) + r_\infty \qquad (11.37)$$

This simple model for a hindered rotor assumes that the decay from r_0 to r_∞ occurs exponentially. More complex expressions may be necessary for a rigorous analysis,[31–33] but the data are rarely adequate to resolve more than one correlation time for a hindered rotation. The constant term r_∞ has been interpreted as resulting from an energy barrier that prevents rotational diffusion of the fluorophore beyond a certain angle. Interpretation of the r_∞ values will be discussed in Section 11.7.

11.4.3. Segmental Mobility of a Biopolymer-Bound Fluorophore

Consider a fluorophore that is bound to a macromolecule, and assume that the fluorophore can undergo segmental motions with a fast correlation time θ_F. Let θ_P be the slow correlation time for overall rotation of the macromolecule. A number of theoretical treatments have appeared.[34–36] These rigorous treatments lead to various expressions for $r(t)$, most of which are well approximated by some simple expressions. Assume the segmental motions of the fluorophore occur independently of the rotational motion of the macromolecules. Then the anisotropy is given by

$$r(t) = r_0\left[\alpha e^{-t/\theta_F} + (1 - \alpha)\right]e^{-t/\theta_P} \qquad (11.38)$$

The anisotropy at any time t depends on the extent of depolarization due to the internal motion with an amplitude $r_0\alpha$ and the extent of depolarization due to overall protein rotation with an amplitude $r_0(1 - \alpha)$. Equation 11.38 may be regarded as a slightly more complex case of the hindered rotor in which the anisotropy decays rapidly to $r_\infty = r_0(1 - \alpha)$ as a result of the segmental motion. However, the anisotropy continues to decay to zero as a result of the overall rotation of the macromolecule. The effect of segmental fluorophore motion within a macromolecule is the appearance of a multi-exponential anisotropy decay. This can be understood by multiplying the terms in eq. 11.38, resulting in two exponentially decaying terms. The faster motion must be hindered ($\alpha < 1$) to observe a multi-exponential decay of $r(t)$. If the segmental motion were completely free, that is, $\alpha = 1$, then the anisotropy would decay with a single apparent correlation time (θ_A). This apparent correlation time would be given by $\theta_A = \theta_P\theta_F/(\theta_P + \theta_F)$. The existence of the segmental motion would only be revealed by the small magnitude of θ_A, relative to the correlation time expected for the macromolecule.

Time-resolved anisotropy decays are usually fit to a sum of exponential decays. Hence, a decay of the form shown by eq. 11.38 is generally fit to

$$r(t) = r_0(f_S e^{-t/\theta_S} + f_L e^{-t/\theta_L}) \qquad (11.39)$$

where the subscripts S and L refer to the short and long correlation times. From comparison of eqs. 11.38 and 11.39 one can derive the following relationships between the parameters:

$$f_S = \alpha, \qquad f_L = (1 - \alpha) \qquad (11.40)$$

$$\frac{1}{\theta_S} = \frac{1}{\theta_F} + \frac{1}{\theta_P}, \qquad \frac{1}{\theta_L} = \frac{1}{\theta_P} \qquad (11.41)$$

Equation 11.41 indicates that it is acceptable to equate the longer correlation time with that of the overall rotational motion. However, the shorter observed correlation time is not strictly equal to the correlation time of the segmental motion. Only when $\theta_F << \theta_P$ is $\theta_S = \theta_F$, the actual correlation time of the fast motion.

The effects of a fast segmental motion on the time-domain and frequency-domain data are shown in Figures 11.6 and 11.7, respectively. The presence of a 50-ps correlation time results in a rapid initial decrease in $r(t)$. The amplitude of this rapid component depends on the amplitude of the motion. In Figure 11.6 this amplitude is assumed to account for half of the total anisotropy ($r_{01} = 0.2$). Following the rapid decrease, the anisotropy decays by the longer correlation time of 5 ns. This is the basis of estimating the overall correlation time of a protein from the correlation time observed at longer times. When the value of θ_F is much less than θ_P, and less than the instrumental resolution, the effect of the fast motion is to decrease the apparent value of r_0. The remaining anisotropy decays with θ_P.

The presence of a short correlation time results in a complex appearance for the FD anisotropy data. The single bell-shaped Δ_ω curve is replaced by a more complex curve (Figure 11.7), which contains contributions from the two correlation times (dashed lines). Depending on the upper frequency limit of the FD instrument, it may not be possi-

ble to measure the maximum values of Δ_ω due to the faster motion. In these cases the observed value of Δ_ω increases up to the highest measured frequency. The presence of a rapid correlation time also results in complex behavior for the modulated anisotropy (r_ω). Depending on the upper frequency limit of the measurement the values of r_ω may not reach the value of r_0.

11.4.4. Correlation Time Distributions

Anisotropy decays can also be analyzed in terms of distributions of correlation times.[37–39] One approach is to describe the correlation time spread in terms of a Gaussian, Lorentzian, or other distribution. The Gaussian (G) and Lorentzian (L) distributions are given by

$$p_G(\theta) = \frac{1}{\sigma\sqrt{2\pi}} \exp\left[-\frac{1}{2}\left(\frac{\theta - \bar{\theta}}{\sigma}\right)^2\right] \tag{11.42}$$

$$p_L(\theta) = \frac{1}{\pi} \frac{\Gamma/2}{(\theta - \bar{\theta})^2 + (\Gamma/2)^2} \tag{11.43}$$

In these expressions θ are the central values, σ the standard deviation of the Gaussian, and Γ the full width at half maximum of the Lorentzian.

Suppose the anisotropy decay is described by a single modal distribution, with a single mean value (θ). That part of the anisotropy that displays a correlation time θ is given by

$$r(t,\theta) = r_0 p(\theta) \exp(-t/\theta) \tag{11.44}$$

where $p(\theta)$ is the probability of a particular correlation time θ. It is not possible to selectively observe the fraction of the anisotropy that decays with θ. Hence, the observed anisotropy decay is given by the integral equation

$$r(t) = r_0 \int_0^\infty p(\theta) \exp(-t/\theta)\, d\theta \tag{11.45}$$

It is also possible to describe the anisotropy decay by a multimodal correlation time distribution. In this case the amplitude that decays with a correlation time θ is given by

$$r(t,\theta) = \sum_j r_{0j} p_j(\theta) \exp(-t/\theta) \tag{11.46}$$

and the observed anisotropy decay is given by

$$r(t) = \sum_j r_{0j} \int_0^\infty p_j(\theta) \exp(-t/\theta)\, d\theta \tag{11.47}$$

In this formulation the distribution shape factors are normalized so that the integrated probability of each mode of the distribution is equal to unity. Equations 11.45 and 11.47 are properly normalized only if none of the probability occurs below zero.[39] Depending on the values of θ, σ, or Γ, part of the probability for the Gaussian or Lorentzian distributions (eqs. 11.42 and 11.43) can occur below zero, even if θ is larger than zero. This component should be normalized by the integrated area of the distribution function above $\theta = 0$. The correlation time distributions can also be obtained using maximum entropy methods, typically without using assumed shapes for the distribution functions.[37–38]

11.4.5. Associated Anisotropy Decays

Multi-exponential anisotropy decay can also occur for a mixture of independently rotating fluorophores. Such anisotropy decay can occur for a fluorophore when some of the fluorophores are bound to protein and some are free in solution. The anisotropy from the mixture is an intensity weighting average of the contribution from the probe in each environment:

$$r(t) = r_1(t) f_1(t) + r_2(t) f_2(t) \tag{11.48}$$

where $r_1(t)$ and $r_2(t)$ are the anisotropy decays in each environment. The fractional time-dependent intensities for each fluorophore are determined by the decay times in each environment. For single exponential decays these fractional contributions are given by

$$f_i(t) = \frac{\alpha_i \exp(-t/\tau_i)}{\alpha_1 \exp(-t/\tau_1) + \alpha_2 \exp(-t/\tau_2)} \tag{11.49}$$

Such systems can yield unusual anisotropy decays that show minima at short times and increase at long times.[40–43] Associated anisotropy decays are described in more detail in Chapter 12.

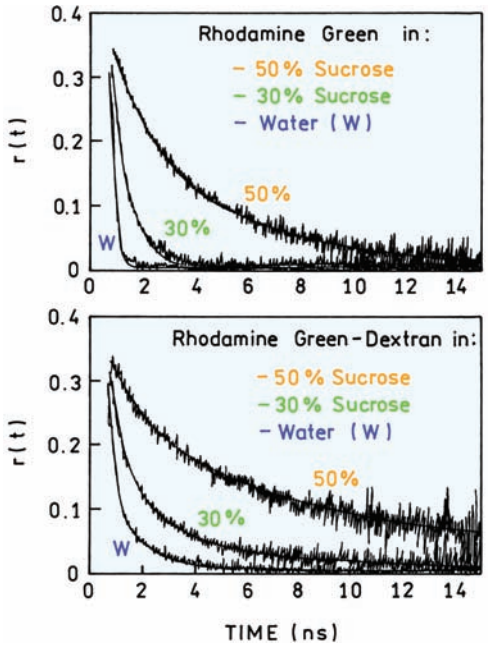

Figure 11.8. Anisotropy decays of Rhodamine Green in water, and 30 and 50% sucrose. Revised from [44].

11.4.6. Example Anisotropy Decays of Rhodamine Green and Rhodamine Green-Dextran

It is instructive to examine several anisotropy decays. Figure 11.8 shows anisotropy decays for rhodamine green (RhG) in water and in water containing high concentrations of sucrose.[44] Water–sucrose mixtures are often used to increase the viscosity of a sample without denaturing the biomolecules. The top panel shows RhG that is not linked to dextran. The anisotropy in water decays in less than a nanosecond. As the viscosity is increased with sucrose the anisotropy decays for slowly, and is discernible from 0 till about 10 ns in 50% sucrose. The lifetimes and correlation times are summarized in Table 11.1. The correlation time in water is 167 ps and increases to 3.44 ns in 50% sucrose. The correlation time increases roughly in proportion to the increase in viscosity. Only a single correlation time was needed to fit the data. The data were collected out to 15 ns, which is about fourfold longer than the RhG lifetime. The upper time limit for measuring the anisotropy data is determined by the intensity decay time of the fluorophore. If the lifetime were longer, then the anisotropy decay data could be collected at longer times.

The lower panel in Figure 11.8 shows the anisotropy decay of RhG when covalently linked to dextran, which had a molecular weight near 10 kDa. The anisotropy decays could not be fit using a single correlation time, but required two correlation times (Table 11.1). The shorter correlation times for RhG–dextran are similar to those found for RhG in water. This suggests the shorter correlation times are due to segmental motions of the covalently bound RhG, and that the motions are similar to the motion of RhG in water. The longer correlation times of RhG–dextran increase with viscosity, but less than expected from the increased in viscosity. For instance, the ratio of the longer correlation times in 50% and 0% sucrose is 6.0, but the ratio of viscosities is 15.4. This result suggests that the segmental motion in RhG–dextran contributed to the longer correlation time shown in eq. 11.38. That is, the longer measured correlation time is shorter than the correlation time for overall rotational diffusion of dextran because of contributions from the segmented motions.

11.5. TIME-DOMAIN ANISOTROPY DECAYS OF PROTEINS

During the past 15 years there have been numerous anisotropy decay measurements on proteins, and it is not practi-

Table 11.1. Anisotropy Decay Parameters for Rhodamine Green and Rhodamine Green-Labeled Dextran[a]

Sample	τ (ns)	r_{01}	θ_1 (ns)	r_{02}	θ_2 (ns)	η/η_ω
Rhodamine Green						
Water	3.94	–	–	0.317	0.167	1.0[b]
30% sucrose	3.85	–	–	0.303	0.721	3.2
50% sucrose	3.70	0	–	0.328	3.44	15.4
Rhodamine Green–dextran conjugate						
Water	3.85	0.226	0.239	0.081	1.99	1.0
30% sucrose	3.68	0.201	0.698	0.114	4.50	3.2
50% sucrose	3.50	0.140	1.94	0.192	12.0	15.4

[a]Revised from [44].
[b]Viscosity (η) relative to the viscosity of water (η_ω).

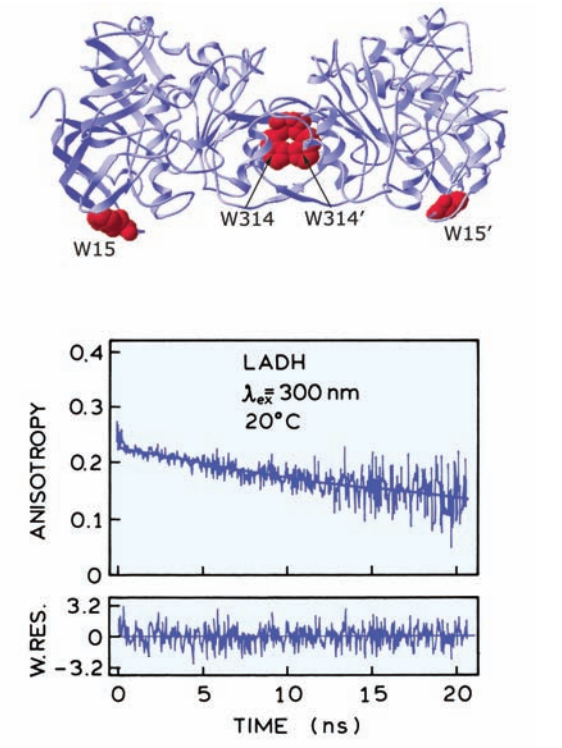

Figure 11.9. Anisotropy decay of LADH excited at 300 nm. The apparent time-zero anisotropy is $r(0) = 0.22$. Revised and reprinted with permission from [45]. Copyright © 1981, American Chemical Society.

cal to even cite the many references. We present examples that illustrate the range of behavior found for proteins.

11.5.1. Intrinsic Tryptophan Anisotropy Decay of Liver Alcohol Dehydrogenase

Liver alcohol dehydrogenase (LADH) is a dimer with two tryptophan residues in each identical subunit and a total molecular weight of 80 kD. One of the residues is exposed to the solvent (trp-15), and one residue is buried (trp-314). This buried residue can be selectively excited on the red edge of the absorption spectrum at 300 nm.[45] The anisotropy decay of LADH excited at 300 nm is shown in Figure 11.9. The decay was found to be a single exponential with a correlation time of 33 ns. This single correlation time can be compared with that predicted for a hydrated sphere (0.2 g H_2O/g of protein and eq. 10.46), which predicts a value of 31 ns at 20°C. Hence this tryptophan residue appears to be rigidly held within the protein matrix.

Trp-314 appears to rotate with the protein, but the data still suggest the presence of some segmental mobility. This is evident from the apparent time-zero anisotropy, $r(0) =$ 0.22, which is less than the fundamental anisotropy of tryptophan at this excitation wavelength. The motions responsible for this loss of anisotropy may be on a timescale faster than the resolution of these measurements. Additionally, the studies have suggested that the apparent correlation times are different with excitation wavelengths. This cannot occur for a sphere, but can occur for non-spherical molecules if different excitation wavelengths change the orientation of the transition in the molecule. LADH is thought to be shaped like a prolate ellipsoid with semi-axes of 11 and 6 nm, and an axial ratio near 1.8.

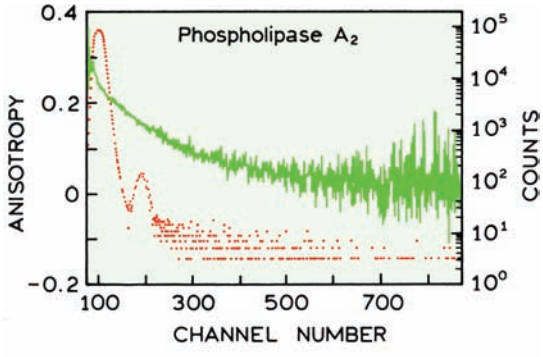

Figure 11.10. Anisotropy decay of trp-3 in phospholipase A_2 30 ps per channel. The anisotropy decay parameters are $r_{01} = 0.104$, $r_{02} = 0.204$, $\theta_1 < 50$ ps and $\theta_2 = 6.5$ ns. Revised from [46].

11.5.2. Phospholipase A_2

A more typical protein anisotropy decay is shown by phospholipase A_2. This enzyme catalyzes the hydrolysis of phospholipids and is most active when located at a lipid-water interface. Phospholipase A_2 has a single tryptophan residue (trp-3), which serves as the intrinsic probe. The anisotropy decay is clearly more complex than a single exponential.[46] At long times the correlation time is 6.5 ns, consistent with overall rotational diffusion. However, in comparison with LADH, there is a dramatic decrease in anisotropy at short times (Figure 11.10). The correlation time of the fast component is less than 50 ps, and this motion accounts for one-third of the total anisotropy.

11.5.3. Subtilisin Carlsberg

The protease Subtilisin Carlsberg (SC) has a single tryptophan residue that is almost completely exposed to water, as seen from an emission maximum of 355 nm, accessibility to quenching by iodide, and the crystal structure (Figure 11.11). The anisotropy decays rapidly to zero with a corre-

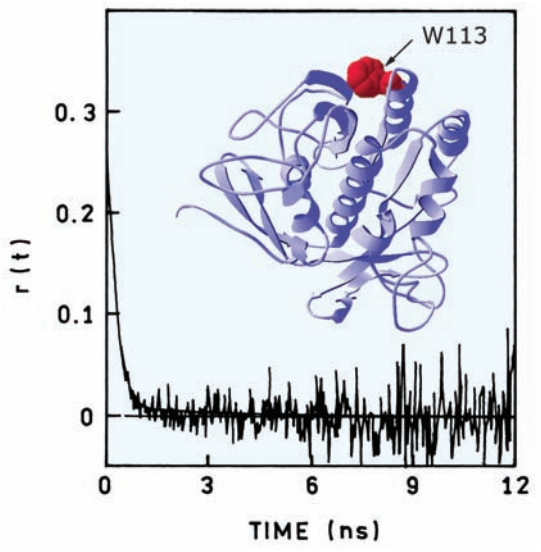

Figure 11.11. Anisotropy decay and structure (insert) of the single-tryptophan side chain in subtilisin Carlsberg. The anisotropy decay parameters are $r(0) = 0.2$, $g_1 = 0.9$, $\theta_1 = 0.17$ ns, $g_2 = 0.1$, and $\theta_2 = 3.5$ ns. Revised from [47].

lation time near 170 ps. There is only a 10% component of a 3.5-ns correlation time that is due to overall rotational diffusion. The correlation time of NATA in water is about 60 ps, so the tryptophan side chain rotates freely relative to the peptide backbone.

Independent tryptophan motions have been observed in a large number of proteins,[48–50] and have been predicted by molecular dynamic calculations.[51] Fast components in the anisotropy decay are also observed for labeled proteins.[52–53] Hence, segmental motions of intrinsic and extrinsic fluorophores appears to be a common feature of proteins.

11.5.4. Domain Motions of Immunoglobulins

Anisotropy decay measurements have been used to examine the flexibility of immunoglobulins in solution.[54–58] Early studies of IgG suggested motions of the F_{ab} fragments that were independent of overall rotational motion. Many immunoglobulins are Y-shaped proteins. The two tops of the Y are the F_{ab} regions that bind to the antigen. In the case of IgE (Figure 11.12) the bottom of the Y is the F_c fragment, which binds to a receptor on the plasma membrane.

In order to study IgE dynamics the antigen dansyl-lysine was bound to the antigen-binding sites on the F_{ab} regions.[59] The anisotropy decays are dramatically different when the IgE is free in solution or when bound to the membrane receptor (Figure 11.13). When bound to the receptor there is a long correlation time of 438 ns (Table 11.2). This correlation time is too long for overall rotational diffusion of the protein, and thus reflects the anisotropy decay of the membrane-bound form of IgE. The actual correlation time is probably longer, because 438 ns was the longest correlation time observable with the 27-ns intensity decay time of the dansyl-lysine.

Domain motions within the IgE molecule are evident from the multi-exponential fits to the anisotropy decays (Table 11.2). When free in solution, IgE displays two corre-

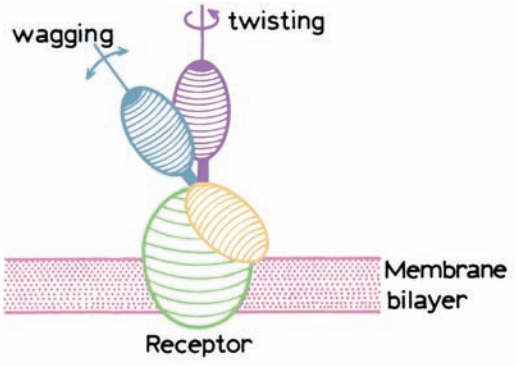

Figure 11.12. Model of IgE complexed with the plasma membrane receptor. The arrows suggest modes of segmental motion of the F_{ab} fragments. Reprinted with permission from [59]. Copyright © 1990, American Chemical Society.

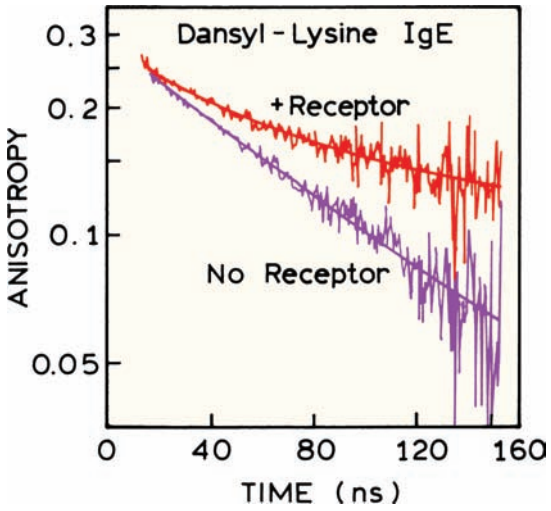

Figure 11.13. Anisotropy decay of dansyl-lysine bound to the antigen binding sites of IgE in the absence and presence of the membrane receptor. Revised and reprinted with permission from [59]. Copyright © 1990, American Chemical Society.

Table 11.2. Anisotropy Decays of Dansyl-Lysine Bound to IgE[a]

Sample	g_1[b]	θ_1 (ns)	g_2	θ_2 (ns)
IgE in solution	0.30	48	0.70	125
IgE receptor	0.32	34	0.68	438

[a]From [59].
[b]The g_j values represent the fraction of the total anisotropy that decay with the correlation time θ_j.

lation times of 48 and 125 ns. The larger value is due to overall rotation of IgE, and the shorter value is due to independent motions of the F_{ab} fragments. Assignment of the 48-ns correlation time to F_{ab} motion is supported by a similar correlation time being present when the antibody bound to the receptor. These results indicate that IgE interacts with its receptor through the F_c region, and that this interaction does not inhibit motion of the F_{ab} domains (Figure 11.12).

11.5.5. Effects of Free Probe on Anisotropy Decays

Anisotropy decays of intrinsic and extrinsic probes frequently show subnanosecond components that are due to rapid segmental motions. However, such components should be interpreted with caution, and can be due to scattered light reaching the detector. Another origin of rapid anisotropy components is the presence of unbound probe in a sample thought to contain only the labeled macromolecule. A free probe will typically display a 50- to 100-ps correlation time, which can easily be mistaken for segmental motion.

The effect of free probe is illustrated by anisotropy decays of the yellow fluorescent protein (YFP) from *Vibrio fischeri*. This protein is from a bioluminescent bacterium, and the emitting fluorophore is flavin mononucleotide (FMN). The intensity decay time of FMN is 4.4 ns in solution and 7.6 ns when bound to YFP. The binding constant of FMN to YFP is only modest, so depending on YFP concentration, some of the FMN can dissociate from the protein.[60]

Anisotropy decays of YFP are shown in Figure 11.14. At higher protein concentration the decay is dominantly due to a 14.8-ns correlation time assigned to overall protein rotation. This correlation is longer than expected for a protein with a molecular weight of 22.7 kD (near 9 ns), which suggests an elongated shape for the protein. It appears the FMN is rigidly bound to YFP. As the protein is diluted, the anisotropy decay shows a fast component near 0.15 ns, which has been assigned to free FMN (Table 11.3). The fast

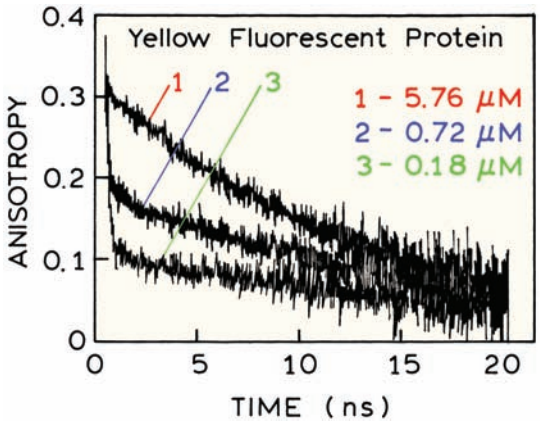

Figure 11.14. Anisotropy decays of yellow fluorescent protein at three concentrations. Revised and reprinted with permission from [60]. Copyright © 1997, American Society for Photobiology.

correlation time is probably beyond the time resolution of the measurements, so that the actual value may be smaller than 0.15 ns. As the protein concentration is decreased, the amplitude of the short decay time (4.4 ns) and the fast correlation time (0.15 ns) increases because a larger fraction of FMN is in the free form. Such data can be used to calculate the dissociation constant of FMN from the protein.

11.6. FREQUENCY-DOMAIN ANISOTROPY DECAYS OF PROTEINS

The frequency-domain method can also be used to resolve the complex anisotropy decays displayed by proteins.[63–67] Examples are provided in Chapter 17, so only a few examples will be presented here.

11.6.1. Apomyoglobin: A Rigid Rotor

Apomyoglobin is known to bind a number of fluorescent probes in its hydrophobic heme binding site. One example is 2-p-toluidinyl-6-naphthalene sulfonate (TNS), which is essentially nonfluorescent in aqueous solution, and becomes highly fluorescent when bound to apomyoglobin. Differential polarized phase angles for TNS-labeled apomyoglobin are shown in Figure 11.15. These values are consistent with a correlation time of 20.5 ns, and an $r(0)$ value of 0.331. Since the r_0 values recovered from the FD data agree with the frozen solution value ($r_0 = 0.32$), these data indicate that TNS-apomyoglobin rotates as a rigid body, without significant free rotation of the TNS group.[67]

Table 11.3. Flavin Mononucleotide Intensity and Anisotropy Decays in the Presence of Yellow Fluorescent Protein (YFP)[a]

[YFP]	α_1[b]	τ_1 (ns)	τ_2 (ns)	r_{01}	θ_1 (ns)	r_{02}	θ_2 (ns)	r[c]
5.76 μM	0.08	4.4	7.6	0.02	0.15	0.29	14.8	0.157
0.72 μM	0.34	"	"	0.17	0.15	0.19	14.8	0.108
0.18 μM	0.69	"	"	0.26	0.14	0.11	14.8	0.071

[a]From [60].
[b]$\alpha_1 + \alpha_2 = 1.0$.
[c]Steady-state anisotropy.

The insert shows the time-resolved anisotropy decay reconstructed from the FD data.

Also shown in Figure 11.15 are FD data for rotational diffusion of TNS in propylene glycol at 20°C. At this temperature the decay time of TNS in propylene glycol is 7.8 ns. The recovered correlation time was 9.5 ns, with $r(0) = 0.351$. As is typical for polar fluorophores in polar solvents, TNS appears to rotate like a spherical molecule.

11.6.2. Melittin Self-Association and Anisotropy Decays

Melittin is a small protein (26 amino acids) that self-associates into tetramers. Melittin was labeled with an anthraniloyl moiety (N-methylanthraniloyl amide, NMA) to serve as an extrinsic probe.[63] Frequency-domain data for the monomeric and tetrameric forms of melittin are shown in Figure 11.16. Also shown are the FD data for the free probe (NMA) not bound to protein. The values of Δ_ω for the free probe are close to zero for all frequencies below 20 MHz, and increased to only several degrees near 150 MHz. Also the modulated anisotropies (r_ω) are near zero at all measurable frequencies. These low values are due to the rapid 73 ps correlation time of the free probe.

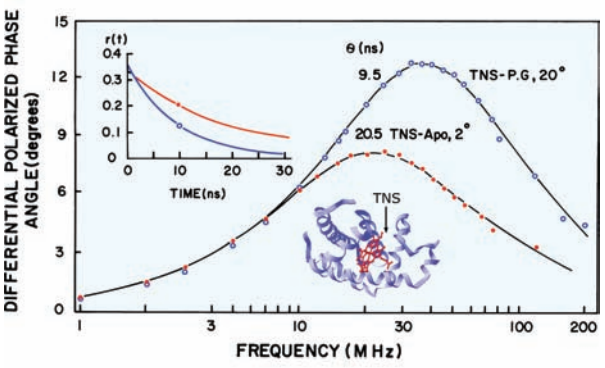

Figure 11.15. Frequency-domain anisotropy decays of 2-p-toluidinyl-6-naphthalene sulfonic acid in propylene glycol (PG) and bound to apomyoglobin (Apo). Insert: TD anisotropy decays. From [67].

The shape of the Δ_ω and r_ω plots are different for the monomer (M) and tetramer (T) forms of melittin. In both cases the anisotropy decays are complex due to significant segmental mobility of the probe with a correlation time near 0.2 ns. Upon formation of a tetramer the shape of the Δ_ω curve shows evidence of overall rotational diffusion with a dominant correlation time near 3.7 ns. In the monomeric state overall rotational diffusion is not visible, but the data contain a substantial component near 1.6 ns, which is due to monomeric melittin. These changes in the overall rate of diffusion upon tetramer formation can be easily seen in the values of r_ω, which are uniformly larger for the tetramer. The frequency-domain data at high frequencies are sensitive to rotational diffusion and local motions of proteins.

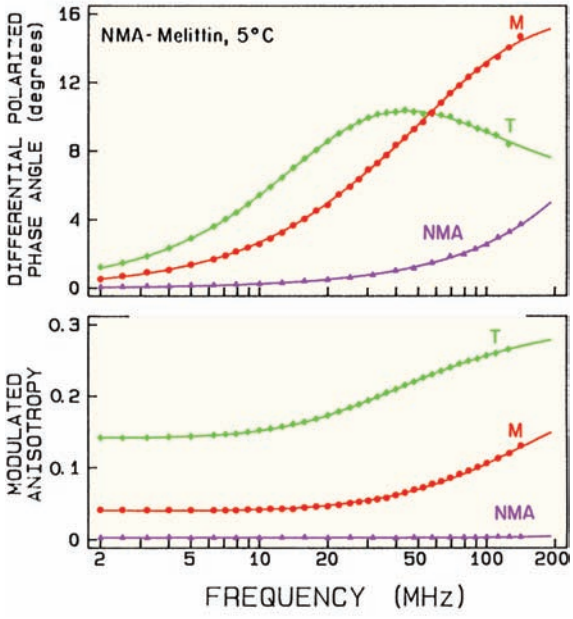

Figure 11.16. Differential phase angles and modulated anisotropies of N-methylanthraniloyl (NMA)-melittin monomer (M) and tetramer (T). Also shown are data for the free probe N-methylanthraniloyl-amide (NMA) at 5°C. Reprinted from [63]. Copyright © 1986, with permission from Elsevier Science.

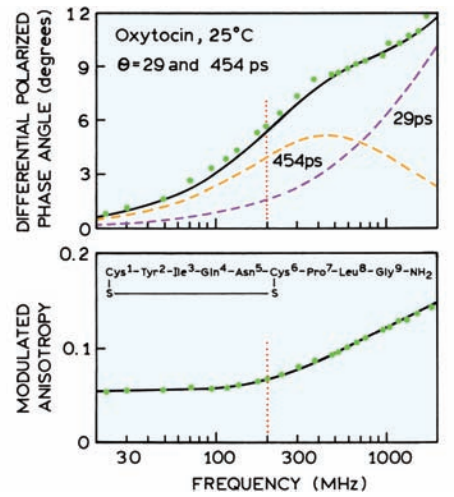

Figure 11.17. Frequency-domain anisotropy decay of the intrinsic tyrosine fluorescence of oxytocin. The dashed curves show the values expected for $r_{01} = 0.208$, $\theta_1 = 29$ ps, $r_{02} = 0.112$, $\theta_2 = 454$ ps. Revised and reprinted from [66]. Copyright © 1986, with permission from Elsevier Science.

11.6.3. Picosecond Rotational Diffusion of Oxytocin

If the correlation times are very short the fast motions can be missed in the measurements. In the time-domain the faster components are resolved by decreasing the width of the instrument response function. In the frequency-domain the resolution of faster components is accomplished by measuring at higher light modulation frequencies (Chapter 5). Measurements to 2 GHz can be used to resolve the picosecond anisotropy decays.

Oxytocin is a small cyclic polypeptide that contains 9 amino acids and a single tyrosine residue. The FD anisotropy decay of the tyrosine fluorescence is shown in Figure 11.17. The FD data to 200 MHz (vertical dotted line) shows only increasing values of Δ_ω and little change in the modulated anisotropy.[66] Hence the data contain incomplete information on the anisotropy decay. This situation is improved by instrumentation which allowed measurements to 2 GHz. In this case there is detectable shape in the values of Δ_ω, and one can see that there are components due to two correlation times, 29 and 454 ps. The 29 ps correlation time is due to segmental motions of the tyrosyl residues, and the 454-ps correlation time is due to overall rotation of the peptide.

11.7. HINDERED ROTATIONAL DIFFUSION IN MEMBRANES

Anisotropy decays can be used to characterize model and real cell membranes. One of the most widely used probes is DPH, originally proposed as a probe to estimate the microviscosity of cell membranes.[68] The basic idea was to compare the anisotropy observed for the membrane-bound probe with that observed for the probe in solutions of known viscosity. By comparison, the microviscosity of the membrane could be calculated. This procedure assumes that the rotational motions are the same in the reference solvent and in the membranes.

A frequently used viscosity reference solvent for DPH is mineral oil. This solvent is used because the decay times of DPH in mineral oil are mostly independent of temperature, whereas the decay times in propylene glycol are dependent on temperature. Polarized intensity decays of DPH are shown in Figure 11.18. In mineral oil the differ-

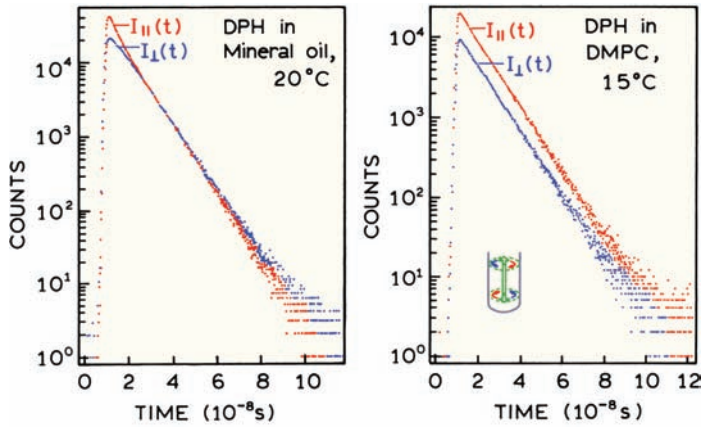

Figure 11.18. Polarized intensity decays of 1,6-diphenylhexatriene (DPH) in mineral oil at 20°C (left) and in DMPC vesicles at 15°C (right). Similar data have been reported from several laboratories.[10,27,30]

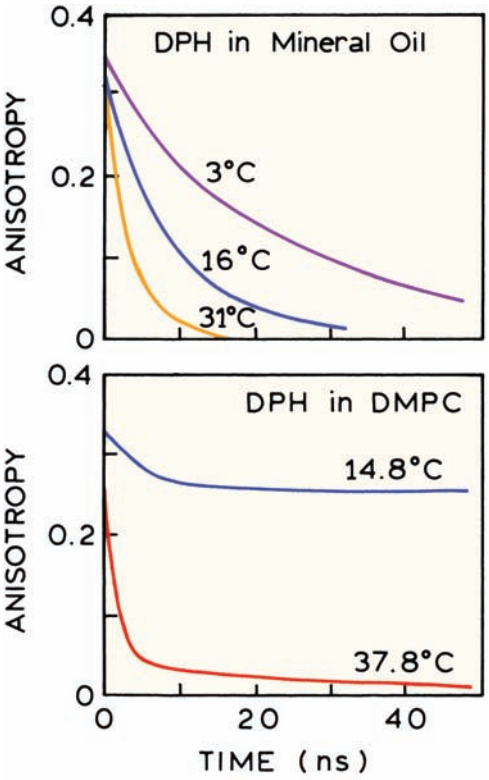

Figure 11.19. Anisotropy decays of DPH in mineral oil and in DMPC vesicles. Redrawn from [10] and [27].

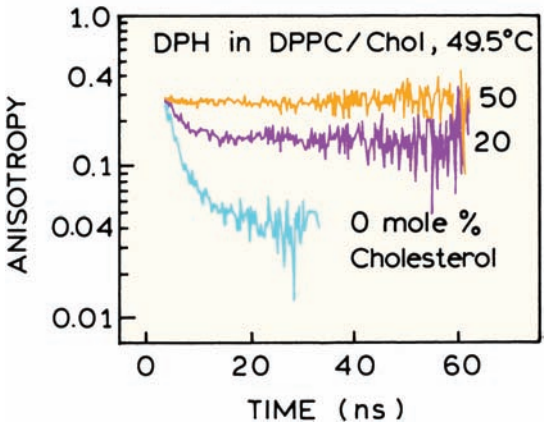

Figure 11.20. Anisotropy decays of DPH in DPPC vesicles at 49.5°C, containing 0, 20, and 50 mole% cholesterol. At 49.5°C the DPPC membranes are above their phase transition temperature, which is near 37°C. Revised and reprinted with permission from [69]. Copyright © 1978, American Chemical Society.

ence decays to zero, indicating the anisotropy decays to zero (left). Contrasting results were found for DPH in vesicles of dimyristoyl-L-α-phosphatidylcholine (DMPC). In this case the polarized intensities remain different during the entire decay (right). This result indicates that the anisotropy does not decay to zero at long times (Figure 11.19). At higher temperature, above the membrane phase transition, the long time anisotropy becomes closer to zero, as shown for DMPC residues at 37.8° (Figure 11.19).

Time-resolved anisotropies can be used to study the effects of cholesterol on membranes. A typical result is that the presence of cholesterol in the membranes results in more hindered rotational diffusion than in the absence of cholesterol. This can be seen in the experimental anisotropy decays of DPH in DPPC vesicles.[69] As the mole fraction of the cholesterol is increased the long time anisotropy increases (Figure 11.20). Such behavior is a general feature of the anisotropy decays of labeled membranes.[70–76]

Considerable attention has been given to the molecular interpretation of the limiting anisotropies (r_∞). The interest arises from a desire to understand the properties of the membranes that are responsible for the hindered rotation. In one analysis[31,77] the rod-like DPH molecule is assumed to exist in a square-well potential so that its rotation is unhindered until a certain angle (θ_c) is reached (see insert in Figure 11.18). Rotation beyond this angle is assumed to be energetically impossible. In this model the limiting anisotropy is related to the cone angle θ_c by

$$\frac{r_\infty}{r_0} = S^2 = \left[\frac{1}{2}\cos\theta_c(1 + \cos\theta_c)\right]^2 \qquad (11.50)$$

This ratio is also equal to the square of the order parameter (S). Completely unhindered motion is found for $\theta_c = 90°$. The limiting anisotropies of DPH can be interpreted in terms of this model. As the cholesterol content of DPPC vesicles increases, the cone angle decreases (Figure 11.21), with the effect being much smaller at higher temperature. The cone angle of DPH in pure DPPC vesicles increases dramatically at the phase transition temperature near 37°C. The presence of cholesterol prevents free rotation of DPH at all temperatures.

This interpretation of the r_∞ values is intuitively pleasing, but the values of θ_c should be interpreted with caution. One difficulty of this model is that the calculation of θ_c from r_∞/r_0 depends upon the existence of a square-well potential in the membranes. The fact that a nonzero value of r_∞ is observed demonstrates the existence of a barrier to rotation, but does not demonstrate the barrier is an abrupt as a square-well potential. For this reason caution is advised in

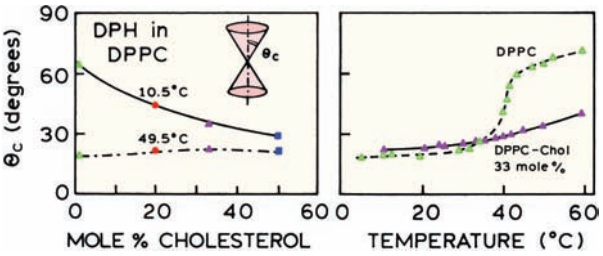

Figure 11.21. Cone angles (eq. 11.50) for rotational diffusion of DPH in DPPC vesicles as a function of the cholesterol content of the vesicles. Revised and reprinted with permission from [69]. Copyright © 1978, American Chemical Society.

the interpretation of derived θ_c values from observed values of r_∞. Alternatively, it has been shown that r_∞ is related to the order parameter describing the equilibrium orientation distribution of the probe at times much longer than the rotational correlation time.[36,78–81] Specifically,

$$S^2 = \frac{r_\infty}{r_0} = \left\langle \frac{3\cos^2\theta - 1}{2} \right\rangle^2 \qquad (11.51)$$

where the brackets indicate an average over all fluorophores, and θ is the angular rotation of DPH in the membrane. This result is claimed to be independent of any assumed model except for the assumption of cylindrical symmetry. In this case $r_\infty = 0$ when the average value of θ reaches 54.7°.

The presence of hindered rotations of DPH results in unusual frequency-domain data.[82–84] The effect of a nonzero value of r_∞ results in a uniform decrease in the differential phase angles (Figure 11.22). The values of Δ_ω are much smaller below the transition temperature of DPPC vesicles,

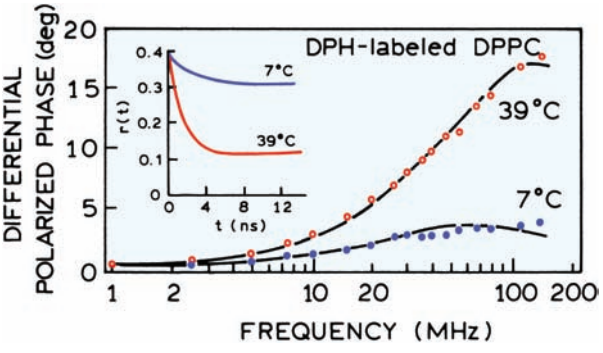

Figure 11.22. Frequency-dependent values of Δ_ω for DPH in DPPC vesicles. The insert shows the recovered anisotropy decay.

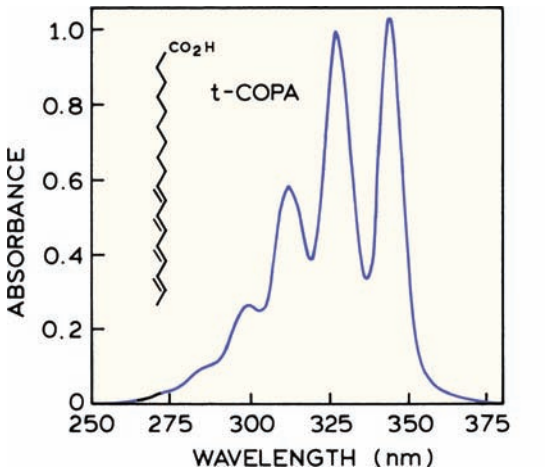

Figure 11.23. Absorption spectra of t–COPA 10^{-6} M in ethanol at 20°C. Revised and reprinted from [85], from the Biophysical Society.

and increases dramatically above the transition temperature, when the DPH molecules can rotate freely. These data can be interpreted using eqs. 11.30–11.34 to recover the time-dependent anisotropy (Figure 11.22, insert).

11.7.1. Characterization of a New Membrane Probe

The concepts described for DPH allow us to understand the characteristics of newly developed probes. One example is the all-trans isomer of 8,10,12,14,16-octadecapentaenoic acid (t-COPA, Figure 11.23). This probe is insoluble and/or nonfluorescent in water, so that the only emission is from t-COPA bound to membranes.[85] The absorption spectrum of t-COPA is centered at 330 nm, making it an acceptor for the intrinsic tryptophan fluorescence of membrane-bound proteins. The effectiveness of t-COPA as an accepted is due to its high extinction coefficient near 105,000 M^{-1} cm^{-1}.

Localization of t-COPA in membranes was accomplished using the spin-labeled fatty acids as quenchers (Chapter 9). DMPC has a phase transition near 24°C, and quenching is more effective in the fluid phase at 30°C than in the gel phase at 17°C (Figure 11.24). The effect of temperature on quenching shows that there is a diffusive component to the quenching, which is in contrast to the usual assumptions of no diffusion in parallax quenching. Larger amounts of quenching by 16NS than by 5NS indicates that the chromophore is buried deeply in the bilayer, away from the lipid-water interface.

The intensity decay of t-COPA is multi-exponential in solvents and in lipid bilayers. In lipids the major component

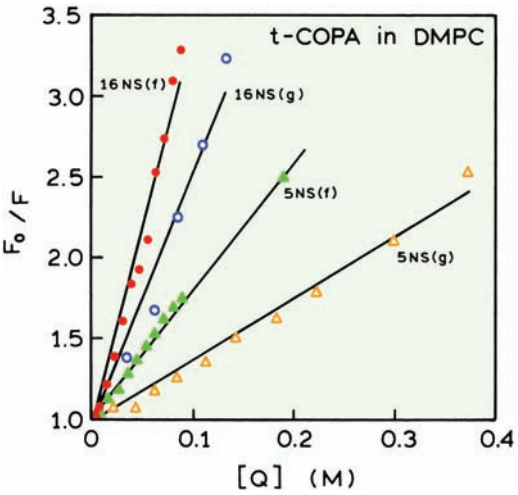

Figure 11.24. Stern-Volmer plot for the quenching of t-COPA by the spin probes 5NS and 16NS in unilamellar vesicles of DMPC at 17°C (gel phase) and 30°C (fluid phase). The concentration refers to the quencher concentration in the membrane phase. Revised and reprinted from [85], from the Biophysical Society.

in the intensity decay has a lifetime of about 20 ns. This means that the anisotropy decay of t-COPA can be measured to longer times than DPH, which has a typically lifetime in membranes near 9 ns. The time-zero anisotropy is near 0.385, making it a useful anisotropy probe. The anisotropy decays of t-COPA are multi-exponential in solvents and in lipid bilayers. In solvents the anisotropy decays to zero (not shown). In membranes t-COPA behaves like a highly hindered rotor. Below the phase transition the anisotropy of t-COPA displays a high r_∞ value near 0.31. Above the phase transition the value of r_∞ decreases to 0.07 (Figure 11.25). In total, this polyene probe behaves similarly to DPH in model membranes.

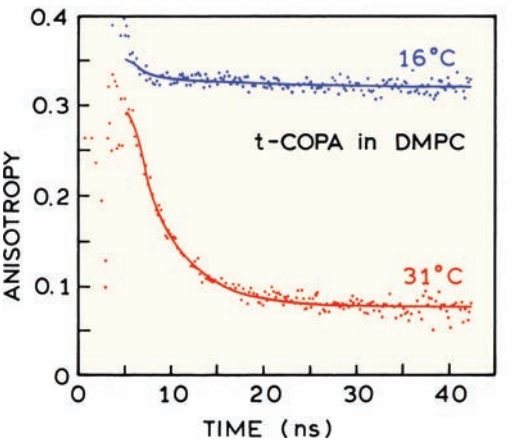

Figure 11.25. Time-resolved fluorescence anisotropy of t-COPA in unilamellar vesicles of DMPC in the gel (16°C) and fluid (31°C) phases. Revised and reprinted from [85], from the Biophysical Society.

11.8. ANISOTROPY DECAYS OF NUCLEIC ACIDS

Studies of DNA by fluorescence can be traced to the use of dyes to stain chromatin for fluorescence microscopy. The use of time-resolved fluorescence for DNA dynamics originated with the measurement of anisotropy decays of ethidium bromide (EB) bound to DNA.[86–89] These early studies showed the anisotropy at long times did not decay to zero (Figure 11.26), which is similar to that found for DPH in membranes. Initially the results were interpreted in terms of the angle through which the EB could rotate within the DNA helix. The anisotropy values in Figure 11.26 are lower than expected for ethidium bromide. This is because the experiments were performed with natural or unpolarized light for the excitation. When the excitation source is unpolarized, the emission is still polarized but the anisotropy values are half those observed with polarized excitation.

Since these early studies there has been theoretical progress in the use of fluorescence to study DNA dynam-

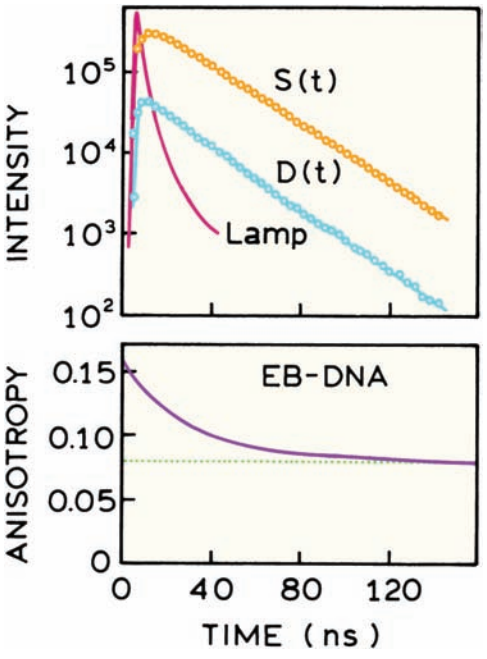

Figure 11.26. Anisotropy decay of ethidium bromide (EB) bound to calf thymus DNA. The excitation was with polarized or natural light. Revised from [86].

ics.[90–92] Unfortunately, the theory for DNA dynamics is rather complex, and not easily summarized. The basic result is that the anisotropy of DNA-bound probes can be depolarized by fast motions of the probes within the DNA helix by bending of DNA about the short axis, and by torsional motion of DNA about the long axis. The extent to which these motions contribute to the anisotropy decay depends on the orientation of the transition moments within the DNA helix. The different motions contribute at different times, and the anisotropy decays are expected to be highly non-exponential. Additional information on DNA anisotropy decays is presented in Chapter 12.

11.8.1. Hydrodynamics of DNA Oligomers

It is easier to interpret the anisotropy decays of short DNA oligomers. These molecules behave like rigid rods allowing the data to be interpreted in terms of the rotational correlation times.[93] The anisotropy of oligomers with up to 32 base pairs decays were found to be single exponentials. The correlation times increased linearly with the number of base pairs (Figure 11.27). Hence, DNA fragments of this size behave as rigid bodies. DNA can adopt shapes besides linear duplexes. One example is formation of bent helices (Figure 11.28). The linear structure (AO) is a DNA 50-mer. The second structure (A5) is bent due to the insertion of five unpaired adenines. This rather modest change in shape cannot be expected to result in a dramatic change in the anisotropy decay. However, the different rotational properties of these two molecules could be seen in the frequency-domain anisotropy data (Figure 11.29). These data were analyzed in terms of a detailed hydrodynamic model, and found to be consistent with the known shapes. The different frequency responses can be understood intuitively by recognizing that the straight DNA molecule can rotate more rapidly around the long axis than the bent molecule. This explains the higher frequency of the maximum differential phase angle of AO (●) as compared to A5 (■). It was possible to detect this minor structural difference between the DNA oligomers from the frequency-domain data.

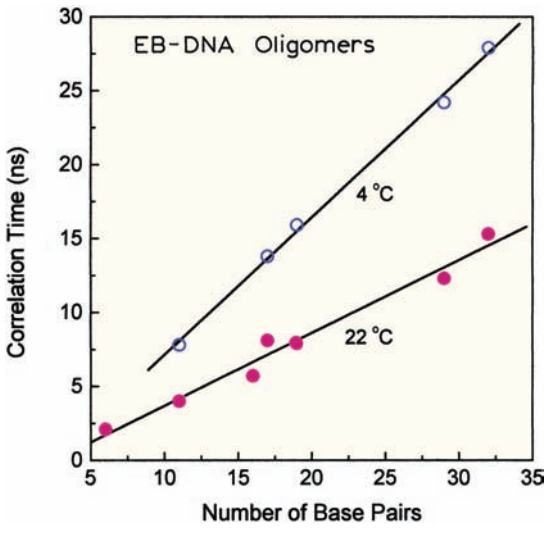

Figure 11.27. Rotational correlation time of EB bound to double helical DNA oligomers as a function of the size of the DNA fragments. Revised and reprinted with permission from [93]. Copyright © 1996, American Chemical Society.

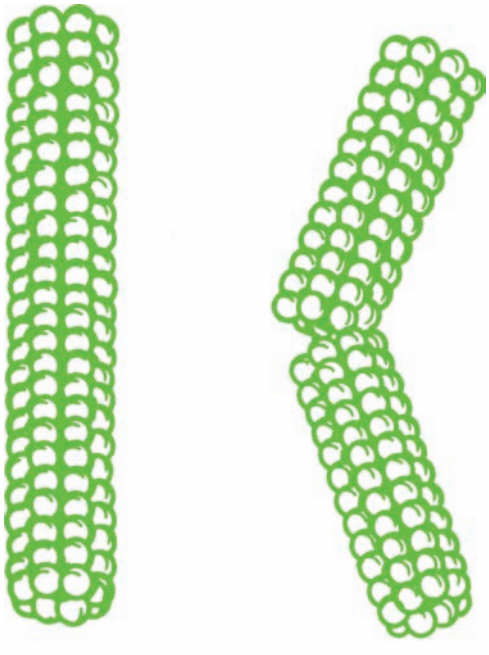

Figure 11.28. Structure of a DNA fragment with 50 base pairs (AO, left) and a bent DNA with five unpaired adenines (A5, right). Reprinted from [94]: Collini M, Chirico G, Baldini G, Bianchi ME, Conformation of short DNA fragments by modulated fluorescence polarization anisotropy, *Biopolymers* **36**:211–225. Copyright © 1995, by permission of John Wiley & Sons, Inc.

11.8.2. Dynamics of Intracellular DNA

During the past ten years there has been an increasing use of time-resolved measurements of a wide variety of intracellular fluorophores. One example is the use of ethidium bromide to study the rigidity of chromatin in Vero monkey kidney cells in the S2 phase.[95] Figure 10.30 (top) shows the intensity decays of EB bound to x-phage DNA as a control, and of EB bound to chromatin in the cells. The intensity

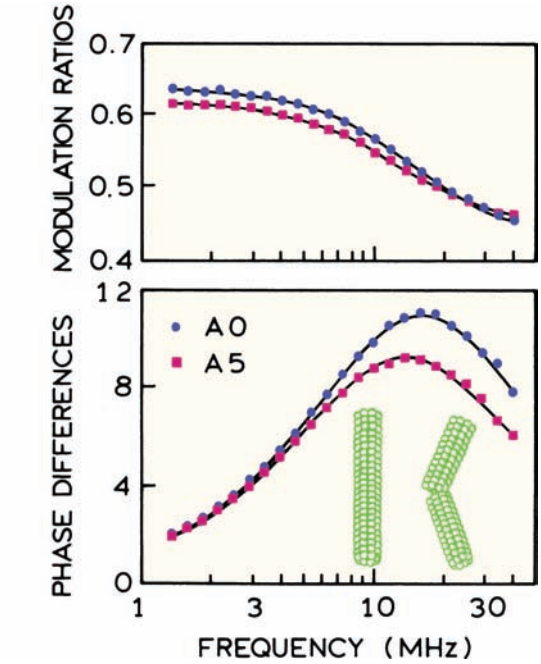

Figure 11.29. Frequency-domain anisotropy decay of the DNA 50-mers shown in Figure 11.28 (AO, ●; A5, ■) labeled with EB. In this figure the modulation data is presented as the ratio of the polarized and modulated intensities, perpendicular divided by parallel. Reprinted from [94]: Collini M, Chirico G, Baldini G, Bianchi ME, Conformation of short DNA fragments by modulated fluorescence polarization anisotropy, *Biopolymers* **36**:211–225. Copyright © 1995, by permission of John Wiley & Sons, Inc.

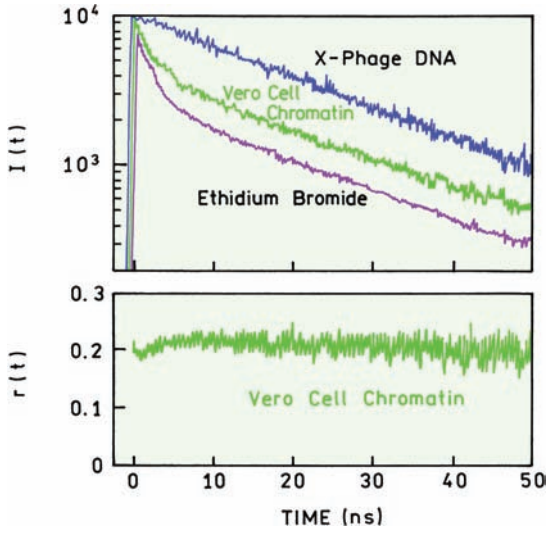

Figure 11.30. Intensity and anisotropy decays of EB-stained chromatin from S2 phase Vero cells. Also shown as a control is the intensity decay of EB bound to x-phage DNA. Revised from [95].

decay of EB bound to x-phage DNA is a single exponential. The intracellular EB shows a short (τ_1 = 2 ns) and a long component (τ_2 = 21 ns). These components were assigned to EB that was not bound or bound to chromatin, respectively. When performing measurements on intracellular probes it is important to determine the binding of the probe as well as the extent of autofluorescence.

The lower panel in Figure 11.30 shows the anisotropy decay of the intracellular EB. The intensity decay is almost flat, showing that the probe is essentially immobile for the 60 ns timescale of the measurements. There is a small dip in the anisotropy near 1–2 ns after excitation. This dip is due to the presence of unbound EB, which rotates rapidly and also decays rapidly. This is an example of an associated anisotropy decay (Section 11.4.5). An important consideration in using a microscope for anisotropy measurements is the numerical aperture of the objective. As the numerical aperture increases the apparent anisotropy (NA) decreases.[96–97] This occurs because light is collected which is not propagating directly along the observation axis. The effect of NA probably contributed to the low apparent value of $r(0)$ in Figure 11.30.

11.8.3. DNA Binding to HIV Integrase Using Correlation Time Distributions

Time-resolved anisotropy decays can be used to measure association reactions between biomolecules. The anisotropy decays in terms of multiple correlation times and the correlation times are assigned to the various species in the samples. It can be difficult to visualize the meaning of a table of correlation times and amplitudes. Part of the difficulty is the tendency to visualize a numerical value as a discrete number, rather than the range of numbers possible because of the limited resolution of the data. A more intuitive approach is to use distributions of correlation times to represent the data.

Correlation time distributions were used to study the interaction of HIV-1 integrase with a DNA substrate. Integrase plays a key role in inserting the viral DNA into the host, and is thus a target for drug therapies. Integrase was known to self-associate and occurs as monomers, dimers, and tetramers.[98–102] Each monomer in integrase has three domains: the N-terminal domain, the catalytic core domain, and the C-terminal domain. The association reactions of integrase and its interaction with DNA are of interest for the design of the anti-HIV drugs. Anisotropy decays of the intrinsic tryptophan emission of integrase were used to

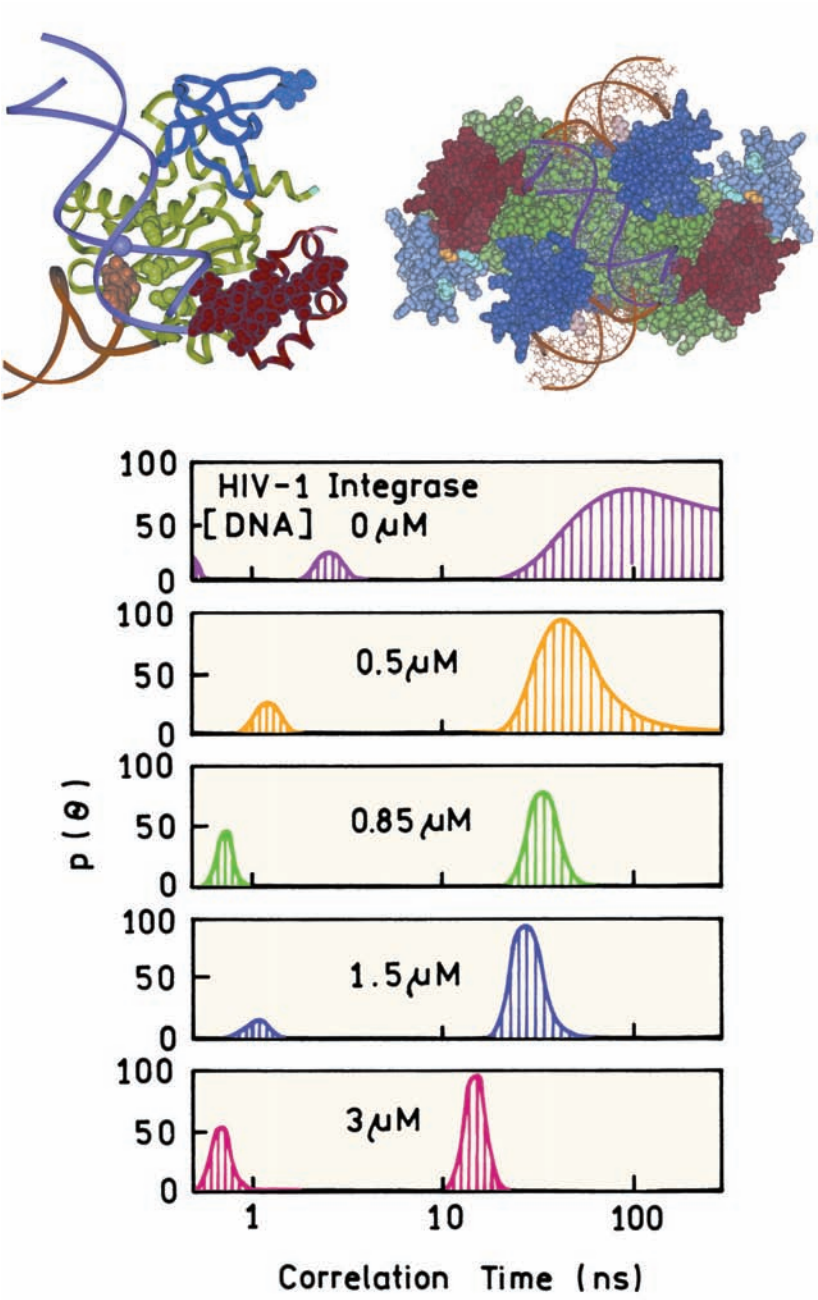

Figure 11.31. Tryptophan correlation time distributions for HIV-1 integrase in the presence of a 21-base-pair DNA oligomer [integrase] = 100 nM. Proposed structures are shown for the monomer and tetramer. N-terminal domain is red, catalytic core domain is green, and the C-terminal domain is blue. Revised from [98–99]. Structure courtesy of Dr. Alexei Podtelezhnikov from the University of California at San Diego.

study the self-association of integrase monomers.[98] Figure 11.31 shows the recovered correlation time distribution for integrase in the absence of DNA substrate. The correlation time near 2–3 ns was assigned to the local dynamics of integrase and not linked to its extent of association. The longer correlation times centered near 100 ns were interpreted as due to the integrase tetramer. The distribution of the long correlation time is wide because this value is uncertain due to the short lifetime of tryptophan. The large difference between the lifetime and correlation time results in the wide amplitude at times above 80 ns which are not determined by the data.

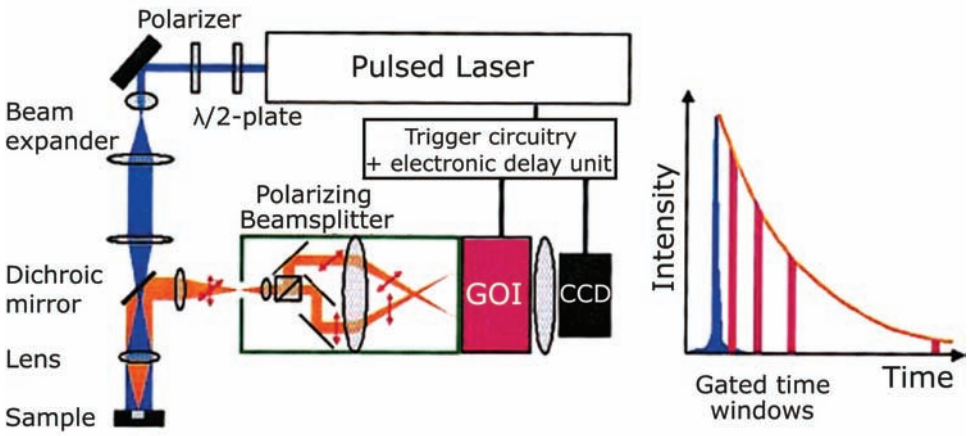

Figure 11.32. Instrument for correlation time imaging. Revised from [105].

Addition of DNA substrate results in a shift of the distribution to shorter time. The correlation time assigned to the monomer is sharply distributed between 10 and 20 ns. The better resolution of this correlation time is because the tryptophan lifetime is closer in magnitude to the correlation time. While the same information would be contained in tabular data, the use of distributions provides an intuitive understanding of both the correlation times themselves and the uncertainties associated with the central values.

11.9. CORRELATION TIME IMAGING

Magnetic resonance imaging (MRI) is a dominant medical imaging technology. The image contrast in MRI is not based on proton signal intensity, but rather on the T_1 and T_2 water or proton relaxation times. The relaxation times depend on the viscosity, elasticity, and other dynamic properties of the tissues, which is similar to the dependence of fluorophore rotational correlation time on solvent viscosity. Here it is natural to ask if cellular imaging can be accomplished based on the rotational correlation times of fluorophores. Such work is beginning to appear,[103–105] and is likely to become more widely used as technology makes these measurements more practical.

An instrument for correlation time imaging is shown in Figure 11.32. This instrument uses a pulsed laser and a gated optical image intensifier (GOI), similar to the instruments described in Chapter 4 for fluorescence lifetime imaging microscopy (FLIM). The instrument shown in Figure 11.32 allows simultaneous recording of the parallel and perpendicular images using a polarizing beam splitter. This optical element separates the image into two images with orthogonal polarizations that are focused on different regions of the CCD camera. Thus a single gating pulse provides two images, one of each polarization, for the same time window.

The correlation time images were measured using rhodamine 6G in transparent microwell plates. The correlation time was varied by using solvents with different viscosities. Figure 11.33 shows the polarized time-dependent decays for R6G in two solvents (right). In methanol the correlation time is short and the polarized intensities are the same at the earliest available times. In ethylene glycol the parallel component has a higher intensity than the perpendicular compo-

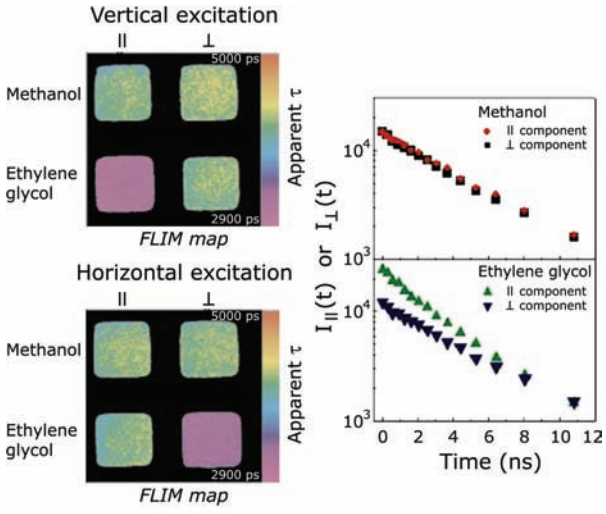

Figure 11.33. Apparent lifetime images (left) and polarized intensity decay (right) for rhodamine 6G in methanol and ethylene glycol. Revised from [105].

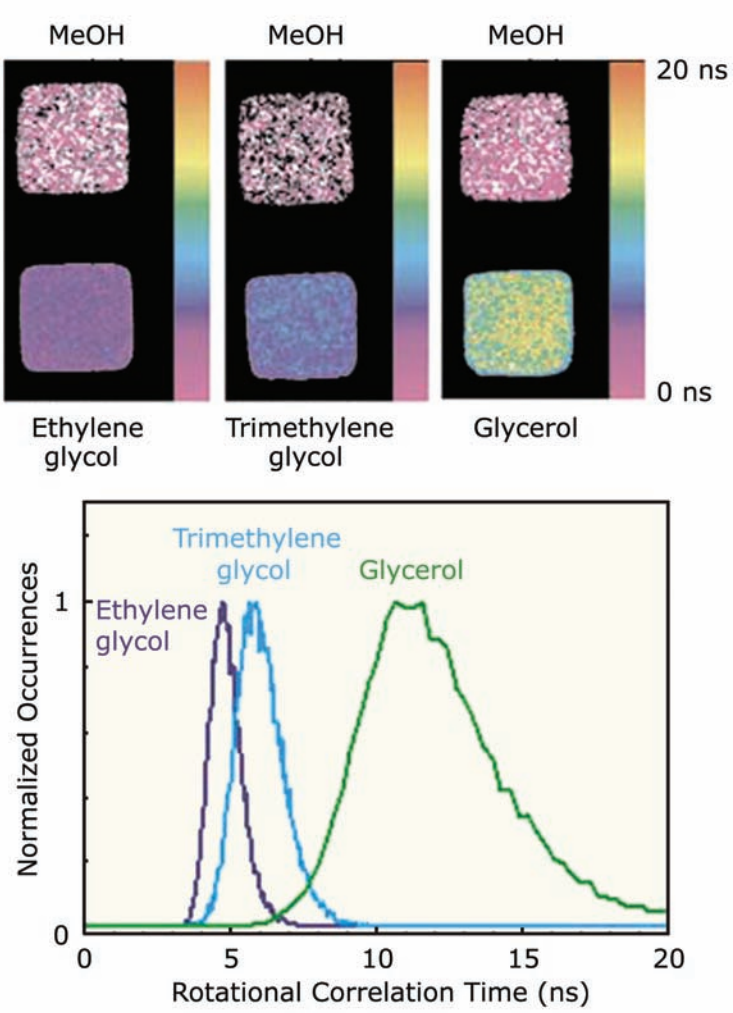

Figure 11.34. Correlation time images of R6G in various solvents (top) and histograms of the recovered correlation times (bottom). The upper three images are R6G in methanol. Revised from [105].

nent to about 6 ns. The polarized intensity decays are visually seen to be multi-exponential as predicted by eqs. 11.1 and 11.2.

The time-dependent decays were used to create FLIM images of the samples (Figure 11.33, left). The lifetimes at each pixel in the images are apparent lifetimes that are some weighted averages of the multi-exponential decays. In methanol the apparent lifetimes are the same regardless of the polarization, as expected based on the short correlation time. In ethylene glycol the apparent lifetime of the parallel component is shorter than the perpendicular component. The parallel component has a shorter apparent lifetime because the transition moments are rotating away from the orientation of the observation polarizer. These results show that the gated polarized intensity images contain information in the correlation times of the samples.

There can be some confusion about the difference in apparent lifetime with horizontal excitation (Figure 11.33, lower left). With the usual right angle geometry horizontal excitation results in the same signals in the parallel and perpendicular channels (Section 10.4). The geometry is different for the instrument in Figure 11.32 where the emission is observed along the same axis as the excitation. For this geometry rotation of the excitation polarizer reverses the signals in the two polarized observation channels.

The polarized time-dependent intensities can be used to calculate the correlation times (Figure 11.34). The color of the images reveals the longer correlation times of R6G in

glycerol as compared to ethylene glycol. The lower panel shows histograms of the occurrence of each correlation time in the examples. While the distribution is wide in glycerol, the results demonstrate the possibility of imaging using correlation times. One can imagine such results being extended to intracellular fluorophores to obtain contrast based on the mobility of fluorophores in each region of a cell.

11.10. MICROSECOND ANISOTROPY DECAYS

11.10.1. Phosphorescence Anisotropy Decays

The information available from an anisotropy decay is limited to times during which emission occurs. For this reason it is usually difficult to obtain reliable data at times longer than three intensity decay times. Even for probes having relatively long lifetimes such as dansyl-lysine (Section 11.5.4), this time window is too small to effectively study membrane-bound proteins.

Rotational motions at longer times can be measured using phosphorescence anisotropy decays.[106–112] These experiments are illustrated by studies of the sarcoplasmic reticulum Ca^{2+}-ATPase, which is a 110-kD transmembrane protein. Not many phosphorescence probes are available, and one of the most commonly used probes is erythrosin (Figure 11.35), which in deoxygenated solution displays a phosphorescence decay time near 100 μs. Typical phosphorescence anisotropy decays are shown for erythrosin-labeled Ca^{2+}-ATPase. In this case the ATPase was aggregated in the membrane by melittin. The extent of aggregation was greater for native melittin than for acetylated melittin, which neutralizes the positive charges on melittin and decreases its interactions with the Ca^{2+}-ATPase. Because the extent of crosslinking is less for acetylated melittin, so that the anisotropy decays more rapidly. There are several disadvantages to the use of erythrosin, eosin and other phosphorescent probes. The signals are usually weak due to the low phosphorescence quantum yields. Rigorous exclusion of oxygen is needed to prevent quenching. And, finally, fundamental anisotropies are usually low, near 0.1, resulting in decreased resolution of the anisotropy decays.

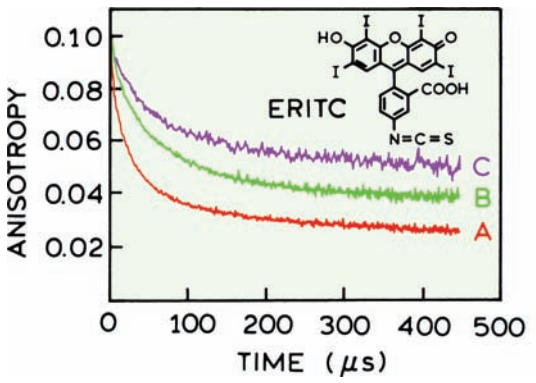

Figure 11.35. Phosphorescence decays of erythrosin-labeled Ca^{2+}-ATPase in sarcoplasmic reticulum vesicles. Anisotropy decays were obtained in the absence of melittin (A), in the presence of acetylated melittin (B), or native melittin (C). Revised and reprinted with permission from [110]. Copyright © 1995, American Chemical Society.

11.10.2. Long-Lifetime Metal–Ligand Complexes

Another approach to measuring long correlation times is to use luminescent metal–ligand complexes (MLCs). These probes display lifetimes ranging from 100 ns to 10 μs[113–116] (Chapter 20). These probes are typically complexes of transition metals with diimine ligands. A lipid MLC probe was made by covalently linking two phosphatidylethanolamine (PE) lipids to an Ru-MLC that contained two carboxyl groups. The MLC-lipid probe was then incorporated into DPPG vesicles (Figure 11.36). The maximum in the differential phase angle (Δ_ω) is near 1 MHz, suggesting slow rotational diffusion. The lifetime of the Ru-PE_2 probe was near

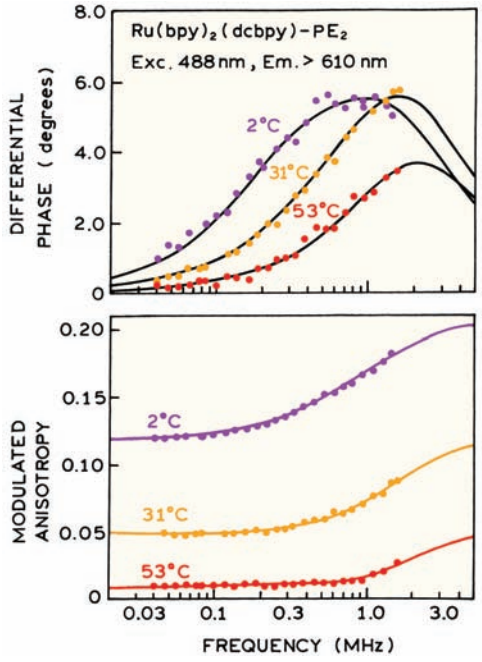

Figure 11.36. Frequency-domain anisotropy decays of $Ru(bpy)_2$ (dcbpy)–PE_2 in DPPG vesicles. Reprinted from [114], with permission from Academic Press, Inc.

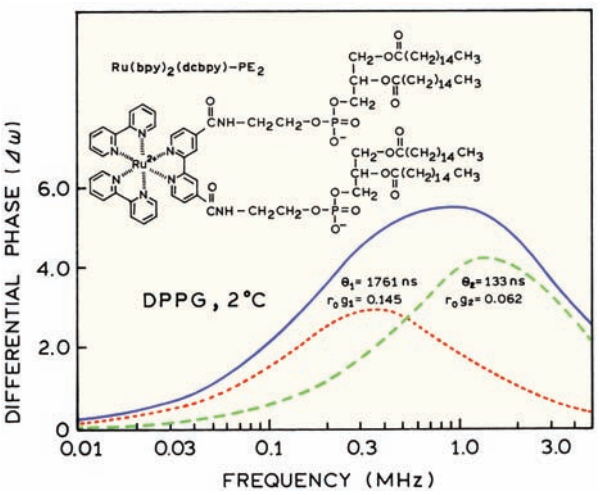

Figure 11.37. Differential phase angles of $Ru(bpy)_2(dcbpy)$–PE_2 in DPPG vesicles at 2°C. The resolution of the Δ_ω values is based on the correlation times and amplitudes shown on the figure. Data from [114].

680 ns at 2°C, which allowed resolution of the slow correlation time.

The FD anisotropy data in Figure 11.37 were used to resolve a double exponential anisotropy decay, which showed correlation times of 133 and 1761 ns. It is useful to visualize how these correlation times contribute to the data, which is shown by the dashed lines in Figure 11.37. The correlation time of 1761 ns is consistent with that expected for rotational diffusion of phospholipid vesicles with a diameter of 250 Å. At this time the physical origin of the shorter correlation time is not clear, but presumably this correlation time is due to restricted motion of the probe within the membrane.

It is important to notice that the use of a long-lifetime probe allowed measurement of overall rotation of the phospholipid vesicles. Earlier in this chapter we saw that DPH displayed nonzero r_∞ values at long times. This occurred because the intensity decay times of DPH are short relative to the correlation times of the vesicles. Hence, the use of nanosecond decay time fluorophores provides no information on rotational motions of lipid vesicles.

The metal–ligand complexes have several advantages over the phosphorescent probes. In contrast to phosphorescence, the samples can be measured in the presence of dissolved oxygen. The MLCs are only partially quenched by ambient oxygen, whereas phosphorescence is usually completely quenched. Additionally, there are relatively few phosphorescent probes, but there are numerous metal–ligand complexes (Chapter 20).

REFERENCES

1. Lakowicz JR, Cherek H, Kusba J, Gryczynski I, Johnson ML. 1993. Review of fluorescence anisotropy decay analysis by frequency-domain fluorescence spectroscopy. *J Fluoresc* **3**(2):103–116.
2. Lakowicz JR, Gryczynski I. 1991. Frequency-domain fluorescence spectroscopy. In *Topics in fluorescence spectroscopy*, Vol. 1: *Techniques*, pp. 293–355. Ed JR Lakowicz. Plenum Press, New York.
3. Spencer RD, Weber G. 1970. Influence of Brownian rotations and energy transfer upon the measurement of fluorescence lifetimes. *J Chem Phys* **52**:1654–1663.
4. Szymanowski W. 1935. Einfluss der Rotation der Molekule auf die Messungen der Abklingzert des Fluoreszenzstrahlung. *Z Phys* **95**: 466–473.
5. Kudryashov PI, Sveshnikov BY, Shirokov VI. 1960. The kinetics of the concentration depolarization of luminescence and of the intermolecular transfer of excitation energy *Opt Spectrosc* **9**:177–181.
6. Bauer RK. 1963. Polarization and decay of fluorescence of solutions. *Z Naturforsch A* **18**:718–724.
7. Cross AJ, Fleming GR. 1984. Analysis of time-resolved fluorescence anisotropy decays. *Biophys J* **46**:45–56.
8. Wahl Ph. 1979. Analysis of fluorescence anisotropy decays by the least squares method. *Biophys Chem* **10**:91–104.
9. Taylor JR. 1982. *An introduction to error analysis*, Vol.. 9, pp. 173–187. University Science Books, Mill Valley, CA.
10. Dale RE, Chen LA, Brand L. 1977. Rotational relaxation of the "microviscosity" probe diphenylhexatriene in paraffin oil and egg lecithin vesicles. *J Am Chem Soc* **252**(21):7500–7510.
11. Papenhuijzen J, Visser AJWG. 1983. Simulation of convoluted and exact emission anisotropy decay profiles. *Biophys Chem* **17**:57–65.
12. Gilbert CW. 1983. A vector method for the non-linear least squares reconvolution-and-fitting analysis of polarized fluorescence decay data. In *Time-resolved fluorescence spectroscopy in biochemistry and biology*, pp. 605–605. Ed RB Cundall, RE Dale. Plenum Press, New York.
13. Beechem JM, Brand L. 1986. Global analysis of fluorescence decay: applications to some unusual experimental and theoretical studies. *Photochem Photobiol* **44**:323–329.
14. Crutzen M, Ameloot M, Boens N, Negri RM, De Schryver FC. 1993. Global analysis of unmatched polarized fluorescence decay curves. *J Phys Chem* **97**:8133–8145.
15. Vos K, van Hoek A, Visser AJWG. 1987. Application of a reference convolution method to tryptophan fluorescence in proteins. *Eur J Biochem* **165**:55–63.
16. Weber G. 1971. Theory of fluorescence depolarization by anisotropic Brownian rotations: discontinuous distribution approach. *J Chem Phys* **55**:2399–2407.
17. Merkelo H, Hammond JH, Hartman SR, Derzko ZI. 1970. Measurement of the temperature dependence of depolarization time of luminescence. *J Luminesc* **1,2**:502–512.
18. Lakowicz JR, Prendergast FG, Hogen D. 1979. Differential polarized phase fluorometric investigations of diphenylhexatriene in lipid bilayers: quantitation of hindered depolarizing rotations. *Biochemistry* **18**:508–519.
19. Reinhart GD, Marzola P, Jameson DM, Gratton E. 1991. A method for on-line background subtraction in frequency domain fluorometry. *J Fluoresc* **1**(3):153–162.

20. Belford GG, Belford RL, Weber G. 1972. Dynamics of fluorescence polarization in macromolecules. *Proc Natl Acad Sci USA* **69**:1392–1393.
21. Chuang TJ, Eisenthal KB. 1972. Theory of fluorescence depolarization by anisotropic rotational diffusion. *J Chem Phys* **57**:5094–5097.
22. Ehrenberg M, Rigler R. 1972. Polarized fluorescence and rotational Brownian diffusion. *Chem Phys Lett* **14**:539–544.
23. Tao T. 1969. Time-dependent fluorescence depolarization and Brownian rotational diffusion of macromolecules. *Biopolymers* **8**: 609–632.
24. Lombardi JR, Dafforn GA. 1966. Anisotropic rotational relaxation in rigid media by polarized photoselection. *J Chem Phys* **44**:3882–3887.
25. Small EW, Isenberg I. 1977. Hydrodynamic properties of a rigid molecule: rotational and linear diffusion and fluorescence anisotropy. *Biopolymers* **16**:1907–1928.
26. Steiner RF. 1991. Fluorescence anisotropy: theory and applications. in *Topics in fluorescence spectroscopy*, Vol. 2: *Principles*, pp. 1–52. Ed JR Lakowicz. Plenum Press, New York.
27. Veatch WR, Stryer L. 1977. Effect of cholesterol on the rotational mobility of diphenylhexatriene in liposomes: a nanosecond fluorescence anisotropy study. *J Mol Biol* **117**:1109–1113.
28. Chen LA, Dale RE, Roth S, Brand L. 1977. Nanosecond time-dependent fluorescence depolarization of diphenylhexatriene in dimyristoyllecithin vesicles and the determination of "microviscosity". *J Biol Chem* **252**(7):2163–2169.
29. Ameloot M, Hendrickx H, Herreman W, Pottel H, Van Cauwelaert F, van der Meer W. 1984. Effect of orientational order on the decay of fluorescence anisotropy in membrane suspensions. *Biophys J* **46**: 525–539.
30. Hildenbrand K, Nicolau C. 1979. Nanosecond fluorescence anisotropy decays of 1,6-diphenyl-1,3,5-hexatriene in membranes. *Biochim Biophys Acta* **553**:365–377.
31. Kinosita K, Kawato S, Ikegami A. 1977. A theory of fluorescence polarization decay in membranes. *Biophys J* **20**:289–305.
32. Kinosita K, Ikegami A, Kawato S. 1982. On the wobbling-in-cone analysis of fluorescence anisotropy decay. *Biophys J* **37**:461–464.
33. Komura S, Ohta Y, Kawato S. 1990. A theory of optical anisotropy decay in membranes. *J Phys Soc Jpn* **59**(7):2584–2595.
34. Wallach D. 1967. Effects of internal rotation on angular correlation functions. *J Chem Phys* **47**:5258–5268.
35. Gottlieb YYa, Wahl Ph. 1963. Étude théorique de la polarisation de fluorescence des macromolecules portant un groupe émetteur mobile autour d'un axe de rotation. *J Chim Phys* **60**:849–856.
36. Lapari G, Szabo A. 1980. Effect of librational motion on fluorescence depolarization and nuclear magnetic resonance relaxation in macromolecules and membranes. *Biophys J* **30**:489–506.
37. Vincent M, Gallay J. 1991. The interactions of horse heart apocytochrome *c* with phospholipid vesicles and surfactant micelles: time-resolved fluorescence study of the single tryptophan residue (Trp-59). *Eur Biophys J* **20**:183–191.
38. Pap EHW, Ter Horst JJ, Van Hoek A, Visser AJWG. 1994. Fluorescence dynamics of diphenyl-1,3,5-hexatriene-labeled phospholipids in bilayer membranes. *Biophys Chem* **48**:337–351.
39. Gryczynski I, Johnson ML, Lakowicz JR. 1994. Analysis of anisotropy decays in terms of correlation time distributions, measured by frequency-domain fluorometry. *Biophys Chem* **52**:1–13.
40. Peng K, Visser AJWG, van Hoek A, Wolfs CJAM, Sanders JC, Hemminga MA. 1990. Analysis of time-resolved fluorescence anisotropy in lipid-protein systems, I: application to the lipid probe octadecyl rhodamine B in interaction with bacteriophage M13 coat protein incorporated in phospholipid bilayers. *Eur Biophys J* **18**:277–283.
41. Visser AJWG, van Hoek A, van Paridon PA. 1987. Time-resolved fluorescence depolarization studies of parinaroyl phosphatidylcholine in triton X-100 micelles and rat skeletal muscle membranes. *Membrane receptors, dynamics, and energetics*, pp. 353–361. Ed KWA Wirtz. Plenum Press, New York.
42. Brand L, Knutson JR, Davenport L, Beechem JM, Dale RE, Walbridge DG, Kowalczyk AA. 1985. Time-resolved fluorescence spectroscopy: some applications of associative behaviour to studies of proteins and membranes. In *Spectroscopy and the dynamics of molecular biological systems*, pp. 259–305. Ed P Bayley, RE Dale. Academic Press, London.
43. Ruggiero A, Hudson B. 1989. Analysis of the anisotropy decay of trans-parinaric acid in lipid bilayers. *Biophys J* **55**:1125–1135.
44. Visser NV, Hink MA, van Hoek A, Visser AJWG. 1999. Comparison between fluorescence correlation spectroscopy and time-resolved fluorescence anisotropy as illustrated with a fluorescent dextran conjugate. *J Fluoresc* **9**(3):251–255.
45. Ross JA, Schmidt CJ, Brand L. 1981. Time-resolved fluorescence of the two tryptophans in horse liver alcohol dehydrogenase. *Biochemistry* **20**:4369–4377.
46. Vincent M, Deveer A-M, De Haas GH, Verheij HM, Gallay J. 1993. Stereospecificity of the interaction of porcine pancreatic phospholipase A_2 with micellar and monomeric inhibitors. *Eur J Biochem* **215**(3):531–539.
47. Lakshmikanth GS, Krishnamoorthy G. 1999. Solvent-exposed tryptophans probe the dynamics at protein surfaces. *Biophys J*, **77**:1100–1106.
48. Deprez E, Tauc P, Leh H, Mouscadot J-F, Auclair C, Brochon J-C. 2000. Oligomeric states of the HIV-1 integrase as measured by time-resolved fluorescence anisotropy. *Biochemistry* **39**:9275–9284.
49. Rami BR, Krishnamoorthy G, Udgaonkar JB. 2003. Dynamics of the core tryptophan during the formation of productive molten globule intermediate of Barstar. *Biochemistry* **42**:7986–8000.
50. Tcherkasskaya O, Ptitsyn OB, Knutson JR. 2000. Nanosecond dynamics of tryptophans in different conformational states of apomyoglobin proteins. *Biochemistry* **39**:1879–1889.
51. Axelsen PH, Gratton E, Prendergast FG. 1991. Experimentally verifying molecular dynamics simulations through fluorescence anisotropy measurements. *Biochemistry* **30**:1173–1179.
52. Fa M, Karolin J, Aleshkov S, Strandberg L, Johansson LB-A, Ny T. 1995. Time-resolved polarized fluorescence spectroscopy studies of plasminogen activator inhibitor type I: conformational changes of the reactive center upon interactions with target proteases, vitronectin and heparin. *Biochemistry* **34**:13833–13840.
53. Broos J, Visser AJWG, Engbersen FJ, Verboom W, van Hoek A, Reinhoudt DN. 1995. Flexibility of enzymes suspended in organic solvents probed by time-resolved fluorescence anisotropy: evidence that enzyme activity and enantioselectivity are directly related to enzyme flexibility. *J Am Chem Soc* **117**(51):12657–12663.
54. Yguerabide J, Epstein HF, Stryer L. 1970. Segmental flexibility in an antibody molecules. *J Mol Biol* **51**:573–590.

55. Hanson DC, Yguerabide J, Schumaker VN. 1981. Segmental flexibility of immunoglobulin G antibody molecules in solution: a new interpretation. *Biochemistry* **20**:6842–6852.
56. Wahl Ph. 1969. Mesure de la décroissance de la fluorescence polarisée de la γ-globuline-1-sulfonyl-5-diméthylaminonaphthlène. *Biochim Biophys Acta* **175**:55–64.
57. Wahl Ph, Kasai M, Changuex J-P. 1971. A study of the motion of proteins in excitable membrane fragments by nanosecond fluorescence polarization spectroscopy. *Eur J Biochem* **18**:332–341.
58. Brochon J-C, Wahl Ph. 1972. Mesures des déclins de l'anisotropic de fluorescence de la γ-globuline et de ses fragments Fab, Fc et $F(ab)_2$ marqués avec le 1-sulfonyl-5-diméthyl-aminonaphthaléne. *Eur J Biochem* **25**:20–32.
59. Holowka D, Wensel T, Baird B. 1990. A nanosecond fluorescence depolarization study on the segmental flexibility of receptor-bound immunoglobulin E. *Biochemistry* **29**:4607–4612.
60. Visser AJG, van Hoek A, Visser NV, Lee Y, Ghisia S. 1997. Time-resolved fluorescence study of the dissociation of FMN from the yellow fluorescence protein from *Vibrio fischeri*. *Photochem Photobiol* **65**(3):570–575.
61. Lakowicz JR, Laczko G, Gryczynski I, Cherek H. 1986. Measurement of subnanosecond anisotropy decays of protein fluorescence using frequency-domain fluorometry. *J Biol Chem* **261**(5): 2240–2245.
62. Maliwal BP, Lakowicz JR. 1986. Resolution of complex anisotropy decays by variable frequency phase-modulation fluorometry: a simulation study. *Biochim Biophys Acta* **873**:161–172.
63. Maliwal BP, Hermetter A, Lakowicz JR. 1986. A study of protein dynamics from anisotropy decays obtained by variable frequency phase-modulation fluorometry: internal motions of N-methylanthraniloyl melittin. *Biochim Biophys Acta* **873**:173–181.
64. Bayley P, Martin S, Browne P, Royer C. 2003. Time-resolved fluorescence anisotropy studies show domain-specific interactions of calmodulin with IQ target sequences of myosin V. *Eur Biophys J* **32**:122–127.
65. Lakowicz JR, Laczko G, Gryczynski I. 1987. Picosecond resolution of tyrosine fluorescence and anisotropy decays by 2-GHz frequency-domain fluorometry. *Biochemistry* **26**:82–90.
66. Lakowicz JR, Laczko G, Gryczynski I. 1986. Picosecond resolution of oxytocin tyrosyl fluorescence by 2-GHz frequency-domain fluorometry. *Biophys Chem* **24**:97–100.
67. Lakowicz JR, Gratton E, Cherek H, Maliwal BP, Laczko G. 1984. Determination of time-resolved fluorescence emission spectra and anisotropies of a fluorophore–protein complex using frequency-domain phase-modulation fluorometry. *J Biol Chem* **259**(17): 10967–10972.
68. Shinitzky M, Barenholz Y. 1978. Fluidity parameters of lipid regions determined by fluorescence polarization. *Biochim Biophys Acta* **515**:367–394.
69. Kawato S, Kinosita K, Ikegami A. 1978. Effect of cholesterol on the molecular motion in the hydrocarbon region of lecithin bilayers studied by nanosecond fluorescence techniques. *Biochemistry* **17**:5026–5031.
70. Kawato S, Kinosita K, Ikegami A. 1977. Dynamic structure of lipid bilayers studied by nanosecond fluorescence techniques. *Biochemistry* **16**:2319–2324.
71. Stubbs CD, Williams BW. 1992. Fluorescence in membranes. In *Topics in fluorescence spectroscopy*, Vol. 3: *Biochemical applications*, pp. 231–271. Ed JR Lakowicz. Plenum Press, New York.
72. Stubbs CD, Kouyama T, Kinosita K, Ikegami A. 1981. Effect of double bonds on the dynamic properties of the hydrocarbon region of lecithin bilayers. *Biochemistry* **20**:4257–4262.
73. Vincent M, de Foresta B, Gallay J, Alfsen A. 1982. Nanosecond fluorescence anisotropy decays of n-(9-anthroyloxy) fatty acids in dipalmitoylphosphatidylcholine vesicles with regard to isotropic solvents. *Biochemistry* **21**:708–716.
74. Pal R, Petri WA, Ben-Yashar V, Wagner RR, Barenholz Y. 1985. Characterization of the fluorophore 4-heptadecyl-7-hydroxycoumarin: a probe for the head-group region of lipid bilayers and biological membranes. *Biochemistry* **24**:573–581.
75. Wolber PK, Hudson BS. 1981. Fluorescence lifetime and time-resolved polarization anisotropy studies of acyl chain order and dynamics in lipid bilayers. *Biochemistry* **20**:2800–2810.
76. Davenport L, Targowski P. 1996. Submicrosecond phospholipid dynamics using a long-lived fluorescence emission anisotropy probe. *Biophys J* **71**:1837–1852.
77. Kinosita K, Kawato S, Ikegami A. 1984. Dynamic structure of biological and model membranes: analysis by optical anisotropy decay measurements. *Adv Biophys* **17**:147–203.
78. Jähnig F. 1979. Structural order of lipids and proteins in membranes: evaluation of fluorescence anisotropy data. *Proc Natl Acad Sci USA* **76**:6361–6365.
79. Heyn MP. 1979. Determination of lipid order parameters and rotational correlation times from fluorescence depolarization experiments. *FEBS Lett* **108**:359–364.
80. Van Blitterswijk WJ, Van Hoeven RP, Van Der Meer BW. 1981. Lipid structural order parameters (reciprocal of fluidity) in biomembranes derived from steady-state fluorescence polarization measurements. *Biochim Biophys Acta* **644**:323–332.
81. Best L, John E, Jähnig F. 1987. Order and fluidity of lipid membranes as determined by fluorescence anisotropy decay. *Eur Biophys J* **15**:87–102.
82. Lakowicz JR, Cherek H, Maliwal BP, Gratton E. 1985. Time-resolved fluorescence anisotropies of diphenylhexatriene and perylene in solvents and lipid bilayers obtained from multifrequency phase-modulation fluorometry. *Biochemistry* **24**:376–383.
83. Faucon JF, Lakowicz JR. 1987. Anisotropy decay of diphenylhexatriene in melittin-phospholipid complexes by multifrequency phase-modulation fluorometry. *Arch Biochem Biophys* **252**(1):245–258.
84. Lakowicz JR. 1985. Frequency-domain fluorometry for resolution of time-dependent fluorescence emission. *Spectroscopy* **1**:28–37.
85. Mateo CR, Souto AA, Amat-Guerri F, Acuña AU. 1996. New fluorescent octadecapentaenoic acids as probes of lipid membranes and protein-lipid interactions. *Biophys J* **71**:2177–2191.
86. Wahl Ph, Paoletti J, Le Pecq J-B. 1970. Decay of fluorescence emission anisotropy of the ethidium bromide–DNA complex evidence for an internal motion in DNA. *Proc Natl Acad Sci USA* **65**(2):417–421.
87. Millar DP, Robbins RJ, Zewail AH. 1981. Time-resolved spectroscopy of macromolecules: effect of helical structure on the torsional dynamics of DNA and RNA. *J Chem Phys* **74**(7):4200–4201.
88. Ashikawa I, Kinosita K, Ikegami A, Nishimura Y, Tsuboi M, Watanabe K, Iso K, Nakano T. 1983. Internal motion of deoxyri-

bonucleic acid in chromatin: nanosecond fluorescence studies of intercalated ethidium. *Biochemistry* **22**:6018–6026.
89. Wang J, Hogan M, Austin RH. 1982. DNA motions in the nucleosome core particle. *Proc Natl Acad Sci USA* **79**:5896–5900.
90. Schurr JM, Fujimoto BS, Wu P, Song L. 1992. Fluorescence studies of nucleic acids: dynamics, rigidities, and structures. in *Topics in fluorescence spectroscopy*, vol. 3: *Biochemical applications*, pp. 137–229. Ed JR Lakowicz. Plenum Press, New York.
91. Thomas JC, Allison SA, Appellof CJ, Schurr JM. 1980. Torsion dynamics and depolarization of fluorescence of linear macromolecules, II: fluorescence polarization anisotropy measurements on a clean viral 29 DNA. *Biophys Chem* **12**:177–188.
92. Barkley MD, Zimm BH. 1979. Theory of twisting and bending of chain macromolecules; analysis of the fluorescence depolarization of DNA. *J Chem Phys* **70**:2991–3007.
93. Duhamel J, Kanyo J, Dinter-Gottlieb G, Lu P. 1996. Fluorescence emission of ethidium bromide intercalated in defined DNA duplexes: evaluation of hydrodynamics components. *Biochemistry* **35**:16687–16697.
94. Collini M, Chirico G, Baldini G, Bianchi ME. 1995. Conformation of short DNA fragments by modulated fluorescence polarization anisotropy. *Biopolymers* **36**:211–225.
95. Tramier M, Kemnitz K, Durleux C, Coppey J, Denjean P, Pansu RB, Coppey-Moisan M. 2000. Restrained torsional dynamics of nuclear DNA in living proliferative mammalian cells. *Biophys J* **78**: 2614–2627.
96. Axelrod D. 1979. Carbocyanine dye orientation in red cell membrane studied by microscopic fluorescence polarization. *Biophys J* **26**:557–574.
97. Axelrod D. 1989. Fluorescence polarization microscopy. *Methods Cell Biol* **30**:333–352.
98. Deprez E, Tauc P, Leh H, Mouscadet J-F, Auclair C, Hawkins ME, Brochon J-C. 2001. DNA binding induces dissociation of the multimeric form of HIV-1 integrase: a time-resolved fluorescence anisotropy study. *Proc Natl Acad Sci USA* **98**(18):10090–10095.
99. Podtelezhnikov AA, Gao K, Bushman FD, McCammon JA. 2003. Modeling HIV-1 integrase complexes based on their hydrodynamic properties. *Biopolymers* **68**:110–120.
100. De Luca L, Pedretti A, Vistoli G, Barreca ML, Villa L, Monforte P, Chimirri A. 2003. Analysis of the full-length integrase-DNA complex by a modified approach for DNA docking. *Biochem Biophys Res Commun* **310**:1083–1088.
101. Leh H, Brodin P, Bischerour J, Deprez E, Tauc P, Brochon JC, LeCam E, Coulaud D, Auclair C, Mouscadet JF. 2000. Determinants of Mg^{2+} -dependent activities of recombinant human immunodeficiency virus type 1 integrase. *Biochemistry* **39**:9285–9294.
102. Deprez E, Tauc P, Leh H, Mouscadet JF, Auclair C, Brochon JC. 2000. Oligomeric states of the HIV-1 integrase as measured by time-resolved fluorescence anisotropy. *Biochemistry* **39**:9275–9284.
103. Suhling K, Siegel J, Lanigan PMP, Lévêque-Fort S, Webb SED, Phillips D, Davis DM, French PMW. 2004. Time-resolved fluorescence anisotropy imaging applied to live cells. *Opt Lett* **29**(6):584–586.
104. Clayton AHA, Hanley QS, Arndt-Jovin D, Subramaniam V, Jovin TM. 2002. Dynamic fluorescence anisotropy imaging microscopy in the frequency domain (rFLIM). *Biophys J*, **83**:1631–1649.
105. Siegel J, Suhling K, Lévêque-Fort S, Webb SED, Davis DM, Phillips D, Sabharwal Y, French PMW. 2003. Wide-field time-resolved fluorescence anisotropy imaging (TR-FAIM): imaging the rotational mobility of a fluorophore. *Rev Sci Instrum* **74**(1):182–192.
106. González-Rodríguez J, Acuña AU, Alvarez MV, Jovin TM. 1994. Rotational mobility of the fibrinogen receptor glycoprotein IIb/IIIa or integrin $\alpha IIb\beta_3$ in the plasma membrane of human platelets. *Biochemistry* **33**:266–274.
107. Lavalette D, Tétreau C, Tourbez M, Blouquit Y. 1999. Microscopic viscosity and rotational diffusion of proteins in a macromolecular environment. *Biophys J* **76**:2744–2751.
108. Lettinga MP, van Kats CM, Philipse AP. 2000. Rotational diffusion of tracer spheres in packings and dispersions of colloidal spheres studied with time-resolved phosphorescence anisotropy. *Langmuir* **16**:6166–6172.
109. Karon BS, Geddis LM, Kutchai H, Thomas DD. 1995. Anesthetics alter the physical and functional properties of the Ca-ATPase in cardiac sarcoplasmic reticulum. *Biophys J* **68**:936–945.
110. Voss JC, Mahaney JE, Thomas DD. 1995. Mechanism of Ca-ATPase inhibition by melittin in skeletal sarcoplasmic reticulum. *Biochemistry* **34**:930–939.
111. Brown LJ, Klonis N, Sawyer WH, Fajer PG, Hambly BD. 2001. Independent movement of the regulatory and catalytic domains of myosin heads revealed by phosphorescence anisotropy. *Biochemistry* **40**:8283–8291.
112. Mueller B, Karim CB, Negrashov IV, Kutchai H, Thomas DD. 2004. Direct detection of phospholamban and sarcoplasmic reticulum Ca-ATPase interaction in membranes using fluorescence resonance energy transfer. *Biochemistry* **43**:8754–8765.
113. Terpetschnig E, Szmacinski H, Lakowicz JR. 1997. Long-lifetime metal–ligand complexes as probes in biophysics and clinical chemistry. *Methods Enzymol* **278**:295–321.
114. Li L, Szmacinski H, Lakowicz JR. 1997. Synthesis and luminescence spectral characterization of long-lifetime lipid metal–ligand probes. *Anal Biochem* **244**:80–85.
115. Guo X-Q, Castellano FN, Li L, Szmacinski H, Lakowicz JR, Sipior J. 1997. A long-lived, highly luminescent Re(I) metal–ligand complex as a biomolecular probe. *Anal Biochem* **254**:179–186.
116. DeGraff BA, Demas JN. 1994. Direct measurement of rotational correlation times of luminescent ruthenium (II) molecular probes by differential polarized phase fluorometry. *J Phys Chem* **98**:12478–12480.

PROBLEMS

P11.1. *Segmental Freedom in Proteins*: Use the data in Figure 11.9 for LADH to calculate the mean angle for the segmental motions of trp-314. Assume the fundamental anisotropy $r_0 = 0.28$.

P11.2. *Binding Constant of FMN for YFP*: Use the intensity decay data in Table 11.3 to calculate the dissociation constant (K_d) of FMN for YFP.